Pergamon

Geochimica et Cosmochimica Acta, Vol. 67, No. 24, pp. 4743–4767, 2003

0016-7037/03 $30.00 + .00

doi:10.1016/S0016-7037(03)00272-2

Polytype distribution of circumstellar silicon carbide: Microstructural characterization by transmission electron microscopy

T. L. DAULTON,[‡1,2,*] T. J. BERNATOWICZ,[3] R. S. LEWIS,[4] S. MESSENGER,[3] F. J. STADERMANN,[3] and S. AMARI[3]

[1]Materials Science Division, Argonne National Laboratory, Argonne IL, 60439-4838, USA
[2]Marine Geosciences Division, Naval Research Laboratory, Stennis Space Center, MS 39529-5004, USA
[3]Laboratory for Space Sciences and Department of Physics, Washington University, St. Louis, MO 63130-4899, USA
[4]Enrico Fermi Institute, University of Chicago, Chicago, IL 60637-1433, USA

(*Received September* 12, 2002; revised 22 April 2003; *accepted in revised form April* 22, 2003)

Abstract—Silicon carbide (SiC) is a particularly interesting species of presolar grain because it is known to form on the order of a hundred different polytypes in the laboratory, and the formation of a particular polytype is sensitive to growth conditions. Astronomical evidence for the formation of SiC in expanding circumstellar atmospheres of asymptotic giant branch (AGB) carbon stars is provided by infrared (IR) studies. However, identification of the crystallographic structure of SiC from IR spectra is controversial. Since >95% of the presolar SiC isolated from meteorites formed around carbon stars, a determination of the structure of presolar SiC is, to first order, a direct determination of the structure of circumstellar SiC. We therefore determined the polytype distribution of presolar SiC from the Murchison CM2 carbonaceous meteorite using analytical and high-resolution transmission electron microscopy (TEM). High-resolution lattice images and electron diffraction of 508 individual SiC grains demonstrate that only two polytypes are present, the cubic 3C (β-SiC) polytype (79.4% of population by number) and the hexagonal 2H (α-SiC) polytype (2.7%). Intergrowths of these two polytypes are relatively abundant (17.1%). No other polytypes were found. A small population of one-dimensionally disordered SiC grains (0.9%), whose high density of stacking faults precluded classification as any polytype, was also observed. The presolar origin of 2H α-SiC is unambiguously established by tens-of-nanometers-resolution secondary ion mass spectroscopy (NanoSIMS). Isotopic maps of a TEM-characterized 2H α-SiC grain exhibit non-solar isotopic compositions of $^{12}C/^{13}C = 64 \pm 4$ and $^{14}N/^{15}N = 575 \pm 24$. These measurements are consistent with mainstream presolar SiC thought to originate in the expanding atmospheres of AGB carbon stars. Equilibrium condensation calculations together with inferred mineral condensation sequences predict relatively low SiC condensation temperatures in carbon stars. The laboratory observed condensation temperatures of 2H and 3C SiC are generally the lowest of all SiC polytypes and fall within the predictions of the equilibrium calculations. These points account for the occurrence of only 2H and 3C polytypes of SiC in circumstellar outflows. The 2H and 3C SiC polytypes presumably condense at different radii (i.e., temperatures) in the expanding stellar atmospheres of AGB carbon stars.

1. INTRODUCTION

Presolar dust grains predate the formation of the solar system, originating in circumstellar outflows and supernovae ejecta. Their widely ranging isotopic compositions reflect nucleosynthetic processes that occurred in the different star types at various stages of stellar evolution. Such dust grains mix into the interstellar medium (ISM) from which subsequent generations of star systems form. As our own protosolar nebula evolved, most of its presolar material was extensively mixed and reprocessed, leading to pervasive isotopic homogeneity that obscured the detailed information concerning the histories and origins of this presolar material. However, some refractory presolar grains survived accretion into primitive bodies and experienced only minimal alteration. Among these grains, those that have isotopic compositions distinct from the average compositions of the solar system in a manner that cannot be produced by mass fractionation, cosmic-ray-induced spallation reactions, or by radioactive decay in situ subsequent to the formation of the solar system can be identified as presolar.

The two most abundant forms of presolar grains isolated from primitive meteorites, diamond (Lewis et al., 1987) and SiC (Bernatowicz et al., 1987; Tang[†] and Anders, 1988), were discovered by tracking the carriers of anomalous noble gas components in density and size separated acid dissolution residues. Presolar SiC is characterized by isotopic anomalies in Si and C (Zinner et al., 1987, 1989; Tang[†] et al., 1989), as well as in minor and trace elements: N (Zinner et al., 1987, 1989), Ne, Xe (Tang[†] and Anders, 1988; Zinner et al., 1989; Lewis et al., 1994), Ar, Kr (Lewis et al., 1994), ^{26}Mg daughters of extinct ^{26}Al (Zinner et al., 1991a), Ca (Amari et al., 2000), Ti (Ireland et al., 1991; Amari et al., 2000), Sr (Podosek et al., 2002), Zr (Nicolussi et al., 1997), Mo (Nicolussi et al., 1998), Ba (Ott and Begemann, 1990; Zinner et al., 1991b; Prombo et al., 1993), Nd, Sm (Zinner et al., 1991b), and Dy (Hoppe and Ott, 1997). The highly anomalous noble gas components, Ne-E(H) and Xe-*s*, led to the discovery of presolar SiC. Xe-*s* isotopes show an enrichment of even-numbered isotopes (^{128}Xe, ^{130}Xe, and ^{132}Xe) and depletion of odd (^{129}Xe, ^{131}Xe), reflecting differences in neutron capture cross sections. They are thought to be produced by *s*-process (slow neutron capture) nucleosynthesis

* Author to whom correspondence should be addressed (tdaulton@nrlscc.navy.mil).
‡ *Present address:* Marine Geosciences Division, Naval Research Laboratory, Stennis Space Center, MS 39529-5004, USA.

(Clayton and Ward, 1978) in low mass (1–3 $M_{\odot}$), thermally pulsing asymptotic giant branch (AGB) stars (Hoppe and Ott, 1997; Gallino et al., 1997) or red giants (Srinivasan and Anders, 1978). Ne-E(H) is a nucleosynthesis product consisting of nearly monoisotopic ^{22}Ne released at high temperatures ($\sim$ 1500 K), characteristic of a refractory carrier. It is distinguished from a similar component, Ne-E(L), released at lower temperatures ($\sim$ 900 K) from a graphite carrier (Amari et al., 1990).

Presolar SiC was first discovered in separates from the Murray CM chondrite (Bernatowicz et al., 1987; Tang† and Anders, 1988), and appears ubiquitous along with the two orders of magnitude more abundant diamond in primitive chondritic meteorites (Huss and Lewis, 1995). Although significantly less abundant, other surviving presolar minerals have been identified: graphite (Amari et al., 1990, 1995a), carbide solid solutions of Ti, V, Fe, Zr, Mo, and Ru (Bernatowicz et al., 1991, 1996, 1999; Croat et al., 2002), kamacite (FeNi) (Bernatowicz et al., 1999), corundum (Al_2O_3) (Hutcheon et al., 1994; Huss et al., 1994; Nittler et al., 1994), spinel ($MgAl_2O_4$) (Nittler et al., 1994), titanium oxide (Nittler and Alexander, 1999), hibonite (Choi et al., 1999), and silicon nitride (Hoppe et al., 1994a, 1996a; Nittler et al., 1995). The relative concentrations of presolar species in meteorites probably reflect variable resistance of different minerals to alteration and not necessarily mineral abundances in the ISM or the abundance of various stellar sources.

Molecular equilibrium condensation models first predicted the condensation of many different mineral species in the atmospheres of AGB carbon stars including SiC (Friedemann, 1969; Gilman 1969), and Woolf and Ney (1969) interpreted excess radiation at infrared (IR) wavelengths from cool stars as thermal emission from circumstellar grains. The first observational evidence of SiC in dusty envelopes of carbon stars came from a relatively broad 11.3 μm IR feature attributed to emission by SiC between the transverse and longitudinal optical phonon frequencies (Treffers and Cohen, 1974; Forrest et al., 1975). Later attempts to identify the crystallographic structure of circumstellar SiC from IR spectra (Blanco et al., 1994, 1998; Groenewegen, 1995; Speck et al., 1997) have generated considerable controversy over the experimental techniques used and the interpretation of the data (Papoular et al., 1998; Speck et al., 1999; Andersen et al., 1999; Mutschke et al., 1999; Henning and Mutschke, 2001).

Astronomical IR spectra were reported to more closely fit α-SiC (hexagonal and rhombohedral) structure (Blanco et al., 1994, 1998; Groenewegen, 1995; Speck et al., 1997) in contrast to, albeit incomplete, meteoritic evidence suggesting that all isotopically anomalous SiC grains have the β-SiC (cubic) structure (Virag et al., 1992). Speck et al. (1999) revised their earlier conclusion (Speck et al., 1997) arguing that inappropriate background matrix corrections (routinely applied to laboratory spectra of KBr-embedded SiC standards) led incorrectly to identification of α-SiC. After removing the background correction, they concluded that β-SiC fit carbon star spectra best (Speck et al., 1999). Although Papoular et al. (1998) demonstrated that matrix effects slant IR-spectral profiles and do not shift resonance features, they argued that profiles could be affected more by grain size and morphology than by polytype structure. Subsequently, Mutschke et al. (1999) reported no systematic dependence of IR-spectral profiles on polytype. Andersen et al. (1999) also reported that variations in the IR spectra among SiC polytypes are smaller than the variations due to grain size, concluding that IR spectroscopy cannot distinguish between polytypes.

Since grain size and microstructure are dependent on physical conditions, such as temperatures and pressures, at which SiC condenses in circumstellar outflows or supernovae ejecta, the outstanding question of polytype is important for understanding conditions where SiC forms. The complexity of interpreting astronomical spectra makes it difficult to determine molecular content, let alone obtain information on chemical processes at sites of grain formation. However, microstructural studies of presolar grains can provide important information about their formation (Bernatowicz et al., 1991, 1996; Daulton et al., 1996). Unfortunately, there are few microstructural studies of meteoritic presolar SiC. Silicon carbide isolated from Murray was reported to be predominantly the cubic polytype (β-SiC) in addition to a few heavily disordered grains (Bernatowicz et al., 1987), although a systematic study of SiC structure was not performed. Virag et al. (1992) examined individual 1.5–26 μm SiC grains from the Murchison L-series separate by Raman spectroscopy and ion probe mass spectroscopy, reporting that all SiC grains exhibiting anomalous isotopic compositions were of the cubic β-SiC structure. However, grains of this size are atypical, comprising less than 0.2% in number and 5% in mass of the total population (Amari et al., 1994). Furthermore, there are numerous reports of grain size dependence of isotopic compositions for Murchison SiC, e.g., ^{14}N/^{15}N (Hoppe et al., 1996a), ^{20}Ne/^{22}Ne, ^{4}He/^{22}Ne (Lewis et al., 1990), ^{80}Kr/^{82}Kr, ^{86}Kr/^{82}Kr (Lewis et al., 1994), ^{50}Ti/^{46}Ti, ^{50}Ti/^{49}Ti (Amari et al., 1996), ^{88}Sr/^{86}Sr (Podosek et al., 2002), and ^{138}Ba/^{136}Ba (Prombo et al., 1993), further emphasizing that the structural characterization by Virag et al. (1992) of the atypical large diameter L-series fraction grains may not be representative of the total presolar SiC population.

Transmission electron microscopy (TEM) is used here to unambiguously determine the distribution of polytypes in presolar SiC grains isolated by acid dissolution from the Murchison CM2 carbonaceous meteorite. In particular, the fine-grained KJB size fraction was examined, because of all KJ series separates it most closely represents the Murchison SiC population. Inasmuch as the population of presolar SiC in primitive meteorites can be regarded as a representative sample of the SiC produced in stellar outflows, the results obtained provide definitive data on the polytype distribution from these outflows to which astronomical measurements and condensation models can be compared. Daulton et al. (2002) presented preliminary results of this work based on analysis of almost half as many presolar SiC grains as described here, but without detailed treatment. Here we present complete results for 508 grains, including a thorough discussion of our experimental techniques and analysis of the SiC crystal structures, as well as a review of previous work on SiC polytype synthesis and the thermodynamics of SiC condensation. In light of these considerations, we then propose a simple hypothesis for circumstellar SiC formation that places the formation of the grains in their proper astrophysical context.

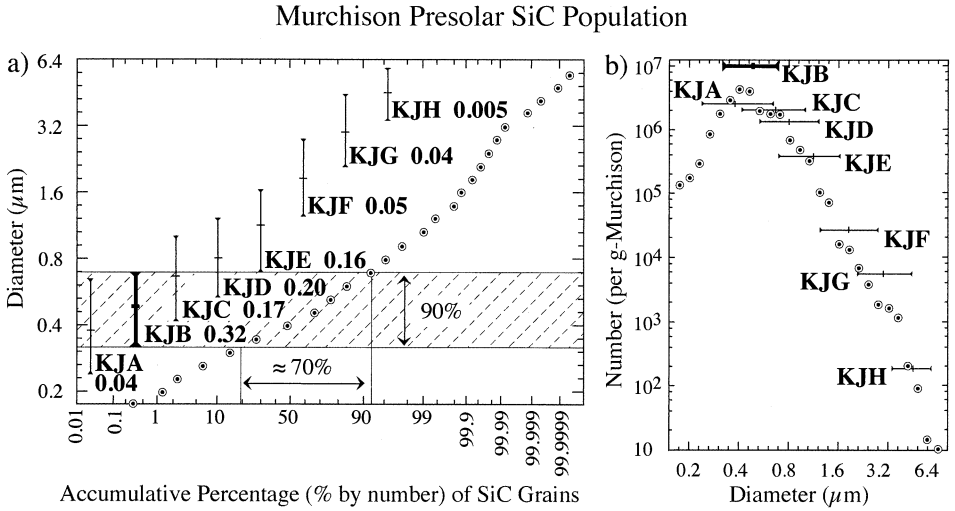

Fig. 1. Size distribution for Murchison SiC grains measured by scanning electron microscopy (Amari et al., 1994), a) accumulative percentage and b) histogram. Circled data points represent size bins that increased by factors of $2^{1/5}$, and are plotted at the top end of each size bin. The dominant size range by number (omitting the 5% tails in either end of distribution) for each size fraction, KJA-KJH, is shown by vertical (a) and horizontal (b) bars with the mean size indicated. The relative mass within each size fraction is indicated by the number next to each size fraction label in (a). The KJB size range is also illustrated by a crosshatched rectangle in (a). The bars are equally spaced in the horizontal direction in (a). In (b), the vertical placement of the bars represents the approximate number density per gram of the separate based on the average SiC grain size and total mass. The ordinate of (a) and the abscissa of (b) are logarithmic with the *n*th mark above and right of 0.2 μm, respectively, having value $10^{-1} \times 2^{(n+5)/5}$ μm. There appears to be an excess of large grains (>2 μm) from that predicted for a log-normal distribution, suggesting the largest grains might be a distinct subpopulation (see Amari et al., 1994).

2. EXPERIMENTAL

2.1. Samples and Instrumentation

2.1.1. Sample preparation

Presolar SiC was isolated from fusion-crust-free fragments of the Murchison (CM2) carbonaceous chondrite by acid dissolution. At one stage of the dissolution process, nanodiamonds were extracted from the residue as a colloid. The resultant greenish-white SiC residue, KJ, was suspended in a 4:1 mixture of isopropanol with H_2O (acidified with HCl), and separated into nine size fractions by centrifugation: KJA (0.24–0.65 μm, mean 0.38μm), KJB (0.32–0.70 μm, mean 0.49μm), KJC (0.42–1.02 μm, mean 0.67μm), KJD (0.54–1.23 μm, mean 0.81 μm), KJE (0.70–1.65 μm, mean 1.14 μm), KJF (1.25–2.79 μm, mean 1.86 μm), KJG (2.11–4.46 μm, mean 3.02 μm), KJH (3.38–5.87 μm, mean 4.57 μm), and KJI (>5 μm). The size ranges quoted are based on scanning electron microscopy (SEM) analysis of grain diameters which omit the 5% tails in either end of the size distributions, while the mean is mass-weighted. The KJB-KJE fractions dominate the mass distribution of the KJ residue. Complete details of the acid dissolution and density separation procedures can be found in Amari et al. (1994).

The KJB separate was chosen for measurement of the distribution of presolar SiC polytypes. Of the nine Murchison size separates, KJB is reported to contain the highest SiC abundance (1.91 ppm of the bulk meteorite corresponding to over 1/3 the mass of SiC) and highest purity (97% SiC) (Amari et al., 1994). Furthermore, KJB is a representative sample of the Murchison SiC population since 70% of the Murchison population lies within 0.3–0.7 μm, characteristic of 90% of the grains in KJB (Fig. 1). Importantly, secondary ion mass spectrometry (SIMS) measurements of individual SiC grains in KJH, KJG, KJF (Hoppe et al., 1994b), KJE (Hoppe et al., 1993, 1996a), KJC (Hoppe et al., 1998), and KJB (Zinner et al., 2001a; Amari et al., 2002) separates indicate that nearly all the grains (>99%) are isotopically anomalous, with enrichments in ^{13}C and ^{14}N relative to solar abundances ($^{12}C/^{13}C = 89$, $^{14}N/^{15}N = 272$). In all SIMS analyses of KJ-series SiC, no isotopically normal (i.e., solar) SiC grains were reported, indicating that these separates contain few SiC grains that are solar nebula products or terrestrial contamination. Nonetheless, isotopic analysis by tens-of-nanometers-resolution SIMS (NanoSIMS) was performed on a TEM microcharacterized SiC grain of interest from the Murchison KJE separate. Specimens for TEM microcharacterization were prepared by ultrasonically suspending the Murchison KJB and KJE SiC residues (separately) in a 1:1 mixture of isopropanol and H_2O. An aliquot (0.5 μL) of the suspension was then directly deposited on 3 mm Cu TEM grids coated with holey amorphous-carbon (a-C) film and allowed to dry. For subsequent NanoSIMS analysis, the perimeter of the Cu TEM grid was secured to a specimen stub with carbon paint.

2.1.2. Transmission electron microscopy

A JEOL JEM-3010 analytical transmission electron microscope, operating at 300 KeV with a LaB_6 filament, an EM-30022 HT pole piece, and a measured point-to-point resolution of 2.1 Å was used for structural microcharacterization. This instrument is equipped with a side-entry motorized 5 axes goniometer, a Noran energy dispersive X-ray spectroscopy (EDXS) system, a Gatan 764 multiscan camera (MSC), and a Gatan imaging filter (GIF200) capable of electron energy loss spectroscopy (EELS). A double-tilt specimen holder allowed tilts of $\pm 45°$ by $\pm 30°$ along orthogonal axes.

All high-resolution (HR)-TEM images were recorded near Scherzer defocus using no objective aperture and the electron optical magnifications were typically 600K–1000K. Lattice image simulations were performed by multislice calculations using the HR-TEM package of the Cerius II lattice modeling software running on a Silicon Graphics Indigo II workstation, and crystallographic analysis was performed using an advanced version of the software package Sphere (Daulton, 1992).

2.1.3. Nanometer-scale secondary ion mass spectrometry

A Cameca NanoSIMS, operating at 16 kV with a Cs^+ ion beam (~1 pA) focused to a probe diameter of 100 nm was used for isotopic compositional imaging. The NanoSIMS has a coaxial, normal-incidence probe (primary) and extraction (secondary) ion-optical system

and was designed for multicollection of mass spectra. The measured spatial resolution of this NanoSIMS is 30 nm for the Cs^+ probe (200 nm for O^-). Five mass-separated secondary ion signals (^{12}C, ^{13}C, $^{12}C^{14}N$, $^{12}C^{15}N$, and ^{30}Si) were acquired in parallel using movable electron multipliers located in a large magnetic sector mass analyzer. High mass resolution was used to completely separate possible interferences. Images were recorded at 256 × 256 pixel resolution with acquisition times of several hours (~ 200 ms/pixel). An optical microscope and secondary electron images were used to position the specimen.

2.2. SiC Polytype Structures

Silicon carbide exhibits an extensive range of well ordered structures. Baumhauer (1912) discovered the first three SiC structures, referring to them as "types," and subsequently coined the term polytype (Baumhauer, 1915). Polytypes of SiC arise from different periodic stacking sequences of bilayers. There are six different bilayers each consisting of two close packed planes (Fig. 2). Bilayers stack to form vertex-sharing tetrahedral cages of Si_4C (or SiC_4) with a C (or Si) atom at the center of each cage. The stacking sequence does not significantly alter bond lengths or affect bulk density (3.2 g-cm^{-3}) (see Tairov and Tsvetkov, 1982). With a Si-C bond distance $\delta = 1.89$ Å, bilayers are spaced 4/3 $\delta \approx 2.52$ Å apart. If the number of bilayers in the unit cell is even, the symmetry must be hexagonal, otherwise it is cubic or rhombohedral. Rather arbitrarily, the rhombohedral and hexagonal classes of SiC polytypes are collectively called α-SiC and the cubic class (consisting of one member) is called β-SiC (Thibault, 1944).

A number of notation schemes are used to describe SiC polytypes. In the Ramsdell (1947) notation, a polytype is denoted by the number of bilayers in the unit cell followed by C, H, or R, denoting the crystal symmetry (i.e., cubic, hexagonal, or rhombohedral). The fundamental bilayers are denoted *bA, cA, aB, cB, aC,* and *bC.* In the earlier Zhdanov (1945) notation, sheet tetrahedra are assigned a positive or negative sense defined by a relative rotation of π radians about the stacking direction (Fig. 2). The successive number of tetrahedral layers, having tetrahedra with a common positive or negative sense, is counted in each subseries present. For example, the polytype denoted 6H (i.e., {. . .*AaBbCcAaCcBb*. . .}) in the Ramsdell notation (Fig. 2) has two subseries each consisting of three tetrahedral layers of the same sense, {· · · +++ −−−. . .}, and in the Zhdanov notation is denoted (33). The polytype denoted 3C (i.e., {. . .*AaBbCc*. . .}) in the Ramsdell notation has an infinite number of tetrahedral layers of the same sense in one subseries, {. . .+. . .}, and is denoted (∞) (Fig. 2). Often SiC polytypes such as 15R (i.e., {. . .*AaBbCcBbAaCcAaBbAaCcBbCcAaCcBb*. . .}) have sequences that repeat {. . .++ − − − ++ − − − ++ − − − · · ·}, denoted (232323), and abbreviated $(23)_3$. Subscripts denoting repeat sequences are nested as in the long periodicity polytype $[(33)_3 6 (33)_5 4]_3$ denoted 174R in the Ramsdell notation. The Zhdanov notation is useful in describing high-resolution lattice images of SiC under defocus conditions that correctly reproduce the projected lattice (Fig. 2). In comparison, the Ramsdell notation is not unique since subscripts are used to distinguish different polytypes with the same notation such as $51R_a$ and $51R_b$ which are uniquely specified in the Zhdanov notation as $[(33)_2 32]_3$ and $[(22)_3 23]_3$. Other polytype notation schemes (Wells, 1950; Jagodzinski, 1954; Wyckoff, 1963) will not be discussed here. On the order of a hundred different SiC polytypes have been reported in the literature (see Verma and Krishna, 1966; Shaffer, 1969), the two most relevant to this work are discussed in detail below.

2.2.1. Hexagonal 2H/(11) α-SiC polytype

The smallest unit cell (lowest order) SiC polytype is hexagonal (space group $P6_3mc$, unit cell lengths $a = 3.08$ Å, $c = 5.03$ Å). This structure is formed by the stacking sequence {. . .*AaBb*. . .}, and is denoted 2H in the Ramsdell notation and (11) in the Zhdanov notation. Hexagonal 2H α-SiC is isostructural to hexagonal 2H diamond (lonsdaleite). It is the only polytype with a 1 in its Zhdanov symbol; in other words, no other polytype contains subsequences of 2H order. Tetrahedra lie in {0001} planes and the 2H stacking sequence of tetrahedral planes is best viewed in HR-TEM images along the $<11\bar{2}0>$ zone axes.

Phase contrast in HR-TEM lattice images is produced by regions of large projected charge density and is highly dependent on instrumental parameters such as defocus, as well as specimen thickness and orientation. In general, the relationship between the image contrast and the atomic structure is not straightforward. Multislice HR-TEM lattice image simulations (e.g., see Cowley and Moodie, 1957) of 2H SiC along $<11\bar{2}0>$ show that a range of image contrast, often differing from the lattice symmetry, is produced depending on defocus (Fig. 3). Under defocus conditions that reflect only the arrangement of the geometric centers of the unresolved Si-C atom pairs, a rectangular array of bright and dark dot contrast is produced. Under defocus conditions that reflect the arrangement of the open channels in the 2H $<11\bar{2}0>$ projected structure, a zigzag bright and dark dot contrast pattern is produced. The zigzag pattern consists of two rhombic arrays that differ in the direction of their major axis. The orientation of the rhombic arrays alternate along the [0001] direction, reflecting the Zhdanov symbol for the structure, (11).

2.2.2. Cubic 3C/(∞) β-SiC polytype

The second smallest unit cell SiC polytype is cubic (space group $F\bar{4}3m$, unit cell length $a = 4.36$ Å). This structure is formed by the stacking sequence {. . .*AaBbCc*. . .} of three bilayers, and is denoted 3C in the Ramsdell notation and (∞) in the Zhdanov notation. Cubic 3C β-SiC is isostructural to cubic 3C diamond and consists of two interpenetrating face-centered cubic (fcc) sublattices, one lattice entirely Si and one entirely C, which are separated by the displacement vector a/4 [111]. Tetrahedra lie in {111} planes and the 3C stacking sequence of tetrahedral planes is best viewed in HR-TEM images along the <011> zone axes.

Unlike 2H SiC and other α-SiC polytypes, HR-TEM lattice images of 3C SiC along <011> exhibit a simple and direct relationship between atomic structure and image contrast. Multi-slice image simulations predict that either the columns of unresolved (400)-spaced C-Si atom pairs or the open channels in the structure are imaged as bright ovals/dots depending on the defocus (Fig. 4). Since the geometric arrangement of these is similar, the predominant change observed in <011> oriented 3C SiC upon varying defocus near the Scherzer condition is a contrast reversal. The 3C polytype does not produce a lattice image under any defocus condition or orientation that is similar to those produced by 2H SiC along $<11\bar{2}0>$ (see Figs. 3 and 4).

2.2.3. Higher order α-SiC polytypes (unit cells larger than 3C)

Lattice images of α-SiC along zone axes perpendicular to the tetrahedral stacking direction and analogous to 3C <011> and 2H $<11\bar{2}0>$ will display a characteristic zigzag contrast pattern reflecting their Zhdanov symbol, under defocus conditions where the symmetry of the open channels in the structure is reproduced. Under such imaging conditions, SiC polytypes are easy to identify from HR-TEM images (Fig. 2). Furthermore, the different polytypes can be readily identified by their electron diffraction patterns (Fig. 2).

2.2.4. Relative abundance of terrestrial SiC polytypes

Natural SiC (moissanite) is a rare terrestrial mineral. It was synthesized before being discovered in nature (Acheson, 1893). The first natural specimens were found in acid residues of the Canyon Diablo meteorite (Moissan, 1905), and these were questioned to be contaminants from synthesized SiC abrasives (Mason, 1967). Numerous early works, particularly in the Russian literature, report the terrestrial occurrence of natural SiC in kimberlites, granitoids as well as in igneous, metamorphic, and sedimentary rocks (for a review see Kaminskiy et al., 1969; Lyakhovich 1980). However, their significance is difficult to evaluate because the question of contamination (see Milton and Vitaliano, 1985) was often not rigorously addressed. Recent studies, however, confirmed the natural occurrence of SiC in mineral concentrates of diamond-bearing kimberlites and lamproites from Fuxian, China (Leung et al., 1990a, 1990b) and Yakutia, Russia (Mathez et al., 1995) as well as in diamond as inclusions (Moore et al., 1986; Moore and Gurney, 1989; Otter and Gurney, 1989; Jaques et al., 1989; Leung 1990).

By far, the most abundant naturally occurring terrestrial SiC reported in the literature is 6H/(33) α-SiC which is followed in abundance by

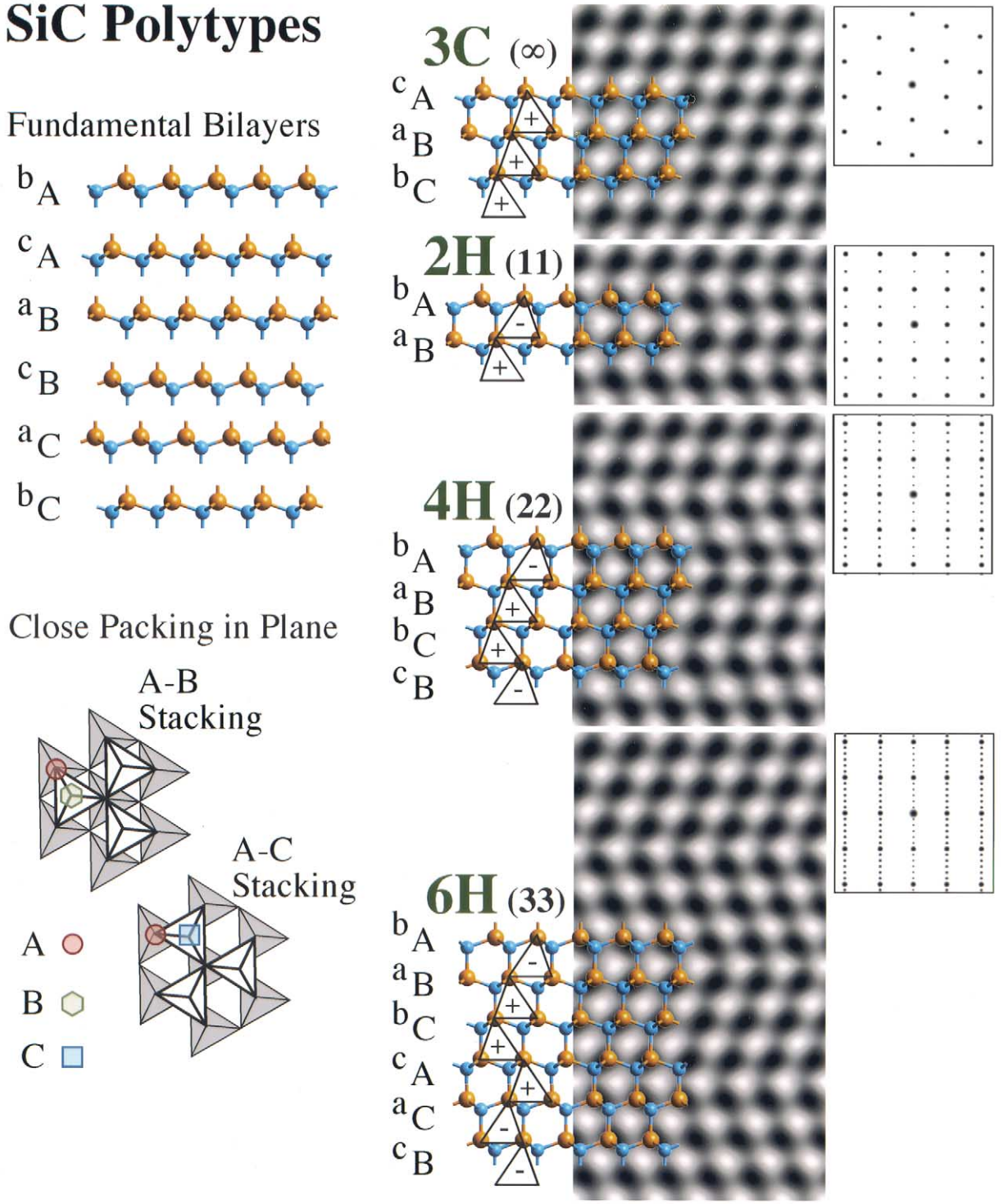

Fig. 2. Silicon carbide polytype structures. Polytypes of SiC are formed by those periodic stacking sequences of bilayers that produce tetrahedral sheets. Atomic models of the six unique (fundamental) bilayers (*bA*, *cA*, *aB*, *cB*, *aC*, and *bC)* of SiC (top left) based on three principle close packed planes (*A*, *B*, and *C*) (lower left) are shown. Blue atoms represent C and orange atoms represent Si. The two basic stacking arrangements, *A-B* and *A-C*, that form planes of vertex-sharing parallel and antiparallel tetrahedra, respectively, are shown (lower left). Atomic models of the four simplest, 3C/(∞), 2H/(11), 4H/(22), and 6H/(33), polytypes are shown superimposed on calculated HR-TEM lattice images produced using defocus conditions that reproduce the symmetry of the projected lattice (center column). Schematic illustrations of diffraction patterns (including forbidden reflections in some cases) are also shown (right column).

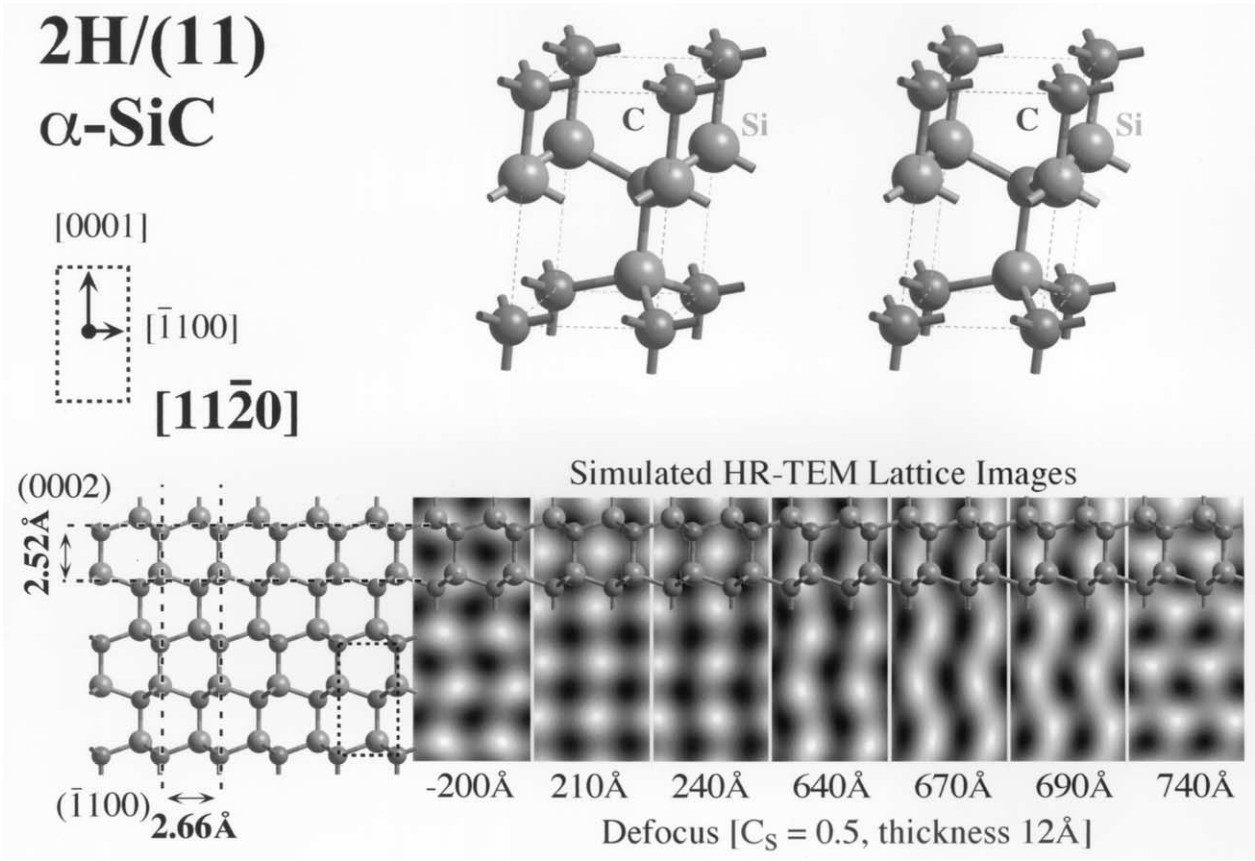

Fig. 3. Atomic models and calculated HR-TEM lattice images of 2H α-SiC. The unit cell is displayed as a stereographic pair (to view using stereographic glasses, reverse the order of the images), and is aligned close to the [1120] direction (top right). The atomic model for the projected [1120] zone axis is shown together with calculated HR-TEM images for a non-inclusive range of defocus conditions (bottom).

$15R/(23)_3$ (often intergrown with 6H) which is followed in abundance by $33R/(3332)_3$. Cubic 3C β-SiC has only been observed as a trace component in the form of inclusions within (Marshintsev et al., 1982) as well as overgrowths on α-SiC found in diamondiferous kimberlites (Leung et al., 1990a, 1990b) and in the form of a mineral within diamond inclusions (Leung, 1990). Marshintsev et al. (1982) reported 3C SiC inclusions in 15R SiC while Leung et al. (1990a, 1990b) and Leung (1990) reported epitaxial overgrowths of 3C SiC on 6H SiC clusters. The only other report of β-SiC (in the salt zone of the Wyoming Green River Formation) is an abstract lacking details (Regis and Sand, 1958). Natural 3C β-SiC is terrestrially extremely rare and natural 2H α-SiC has *never* been reported forming terrestrially.

Large-scale commercial SiC (Carborundum) is produced by heating carbon and silica together with sawdust and salt (to assist in escape of evolved CO gases and convert impurities into volatile chlorides, respectively) in an electric furnace up to 3000 K (method of Acheson, 1893). The most abundant SiC polytype produced by the Acheson process is 6H followed by 15R and 4H/(22) (Verma and Krishna, 1966). Both 3C and 2H SiC are generally not recovered in significant amounts from this process since both are reported to transform irreversibly at high temperature to the 6H polytype via 2H -> 3C -> 6H (Krishna et al., 1971; Krishna and Marshall, 1971a; Bootsma et al., 1971) and 2H–> 6H (Krishna and Marshall, 1971b).

Many processes have been developed to synthesize SiC with higher elemental and polytype purity: crystallization from solution, C implantation into Si substrates, and forms of vapor condensation known in the literature as sublimation (Lely method; Lely, 1955), seeded sublimation (modified Lely method; Tairov and Tsvetkov, 1978), gaseous cracking, chemical vapor deposition (CVD), as well as molecular beam epitaxy (MBE). All together, these processes synthesize on the order of a hundred different SiC polytypes that, however, are not exploited commercially at a significant scale yet. *Therefore, only 6H, 15R, and 4H SiC have significant potential as terrestrial contaminants in meteorite specimens, and the following section shows their abundance is constrained to be <0.2% by number in Murchison KJB.*

3. RESULTS

3.1. Microstructural Characterization of Presolar SiC

The distribution of SiC polytypes present in the circumstellar outflows was determined from TEM measurements of over 508 randomly selected grains in the Murchison KJB separate. Sample deposition on a-C TEM support films deposits the grains in random orientations, often in clusters. Only isolated, individual SiC grains were examined. The diameters of the analyzed grains (defined as the square root of their projected area) ranged from 0.18 to 0.39 μm (omitting the 5% tails in either end of the size distribution) with a mean of 0.27 μm. It should be noted that the TEM and SEM (Amari et al., 1994) size measurements cannot be directly compared because of a number of factors such as resolution, differences in sample deposition, and attrition losses of the original separate over the years.

The structure of a crystal, or in this case polytype, can be determined by analysis of selected area electron diffraction (SAED) patterns, convergent beam electron diffraction

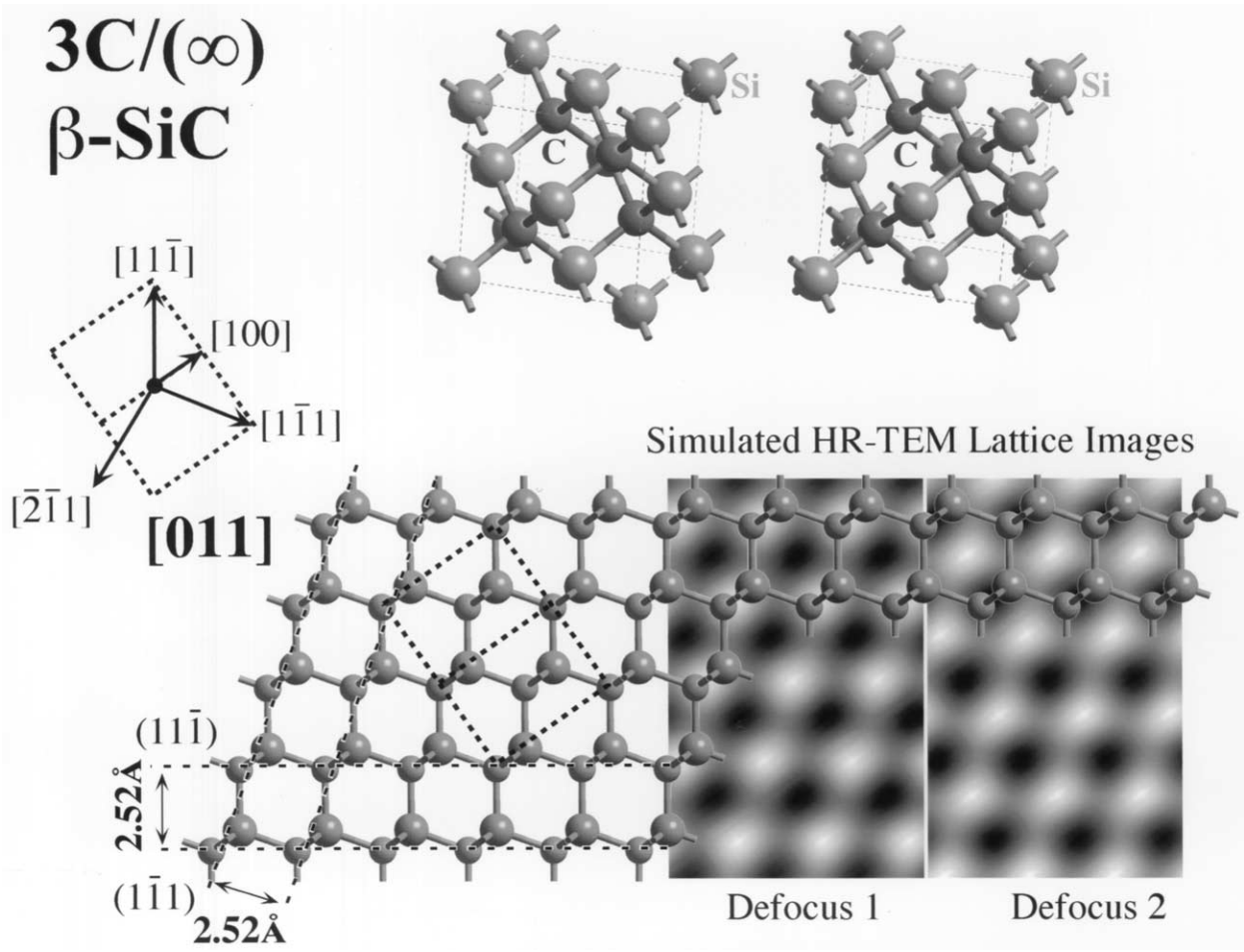

Fig. 4. Atomic models and calculated HR-TEM lattice images of 3C β-SiC. The unit cell is displayed as a stereographic pair (to view using stereographic glasses, reverse the order of the images), and is aligned close to the [100] direction (top right). The atomic model for the projected [011] zone axis is shown together with calculated HR-TEM images from two representative defocus conditions (bottom).

(CBED) patterns, and HR-TEM lattice images from a set of crystallographic directions. Together with a crystallographic analysis of the relative orientations of the different high symmetry zone axes, the structure of a crystal can be well determined. However, such analyses are time prohibitive for the large number of grains examined in this study. Therefore, identification of polytype was performed by the most straightforward methods, namely from SAED patterns and HR-TEM lattice images recorded along a low-index zone axis perpendicular to the tetrahedral stacking direction of a grain.

Kikuchi bands, imaged by CBED, were used to guide tilting of the grains to suitable zone axes. The average crystal structure was determined by SAED from the entire grain while local structure within a grain was determined by SAED from small regions of the grain. High-resolution lattice images recorded from thin areas were used to further characterize the grain microstructure. The position of each grain examined and the tilt angles used were recorded to insure that no grain was analyzed twice.

Lattice images and SAED patterns demonstrate that only two SiC polytypes are present in KJB: cubic 3C β-SiC and hexagonal 2H α-SiC. Grains exhibiting epitaxial intergrowth of these two polytypes were also present. A small number of one-dimensionally disordered SiC grains that could not be classified as any polytype were also observed. No other SiC polytypes were observed out of the over 508 individual grains examined.

3.1.1. Microstructure of presolar 3C β-SiC

All 3C β-SiC grains showed varying concentrations of stacking faults along the <111> directions. A fraction of the 3C SiC grains possessed "rotational" disorder about the <011> axis evident in their diffraction patterns by the presence of slightly arced {111} Bragg reflections and diffuse Kikuchi bands. The origin of this disorder is discussed later. Single crystals of 3C SiC were the most commonly observed grains. However, many 3C SiC grains were multiply twinned (Fig. 5) with double diffraction present in the SAED patterns, complicating polytype identification.

One of the lowest energy interfaces in SiC corresponds to twinning across close-packed tetrahedral planes. This twin structure results when the stacking sequence is abruptly reversed, e.g., {*AaBb*C*c*B*b*A*a*}, by the introduction of a stacking fault. In coincident site lattice (CSL) notation, this twin struc-

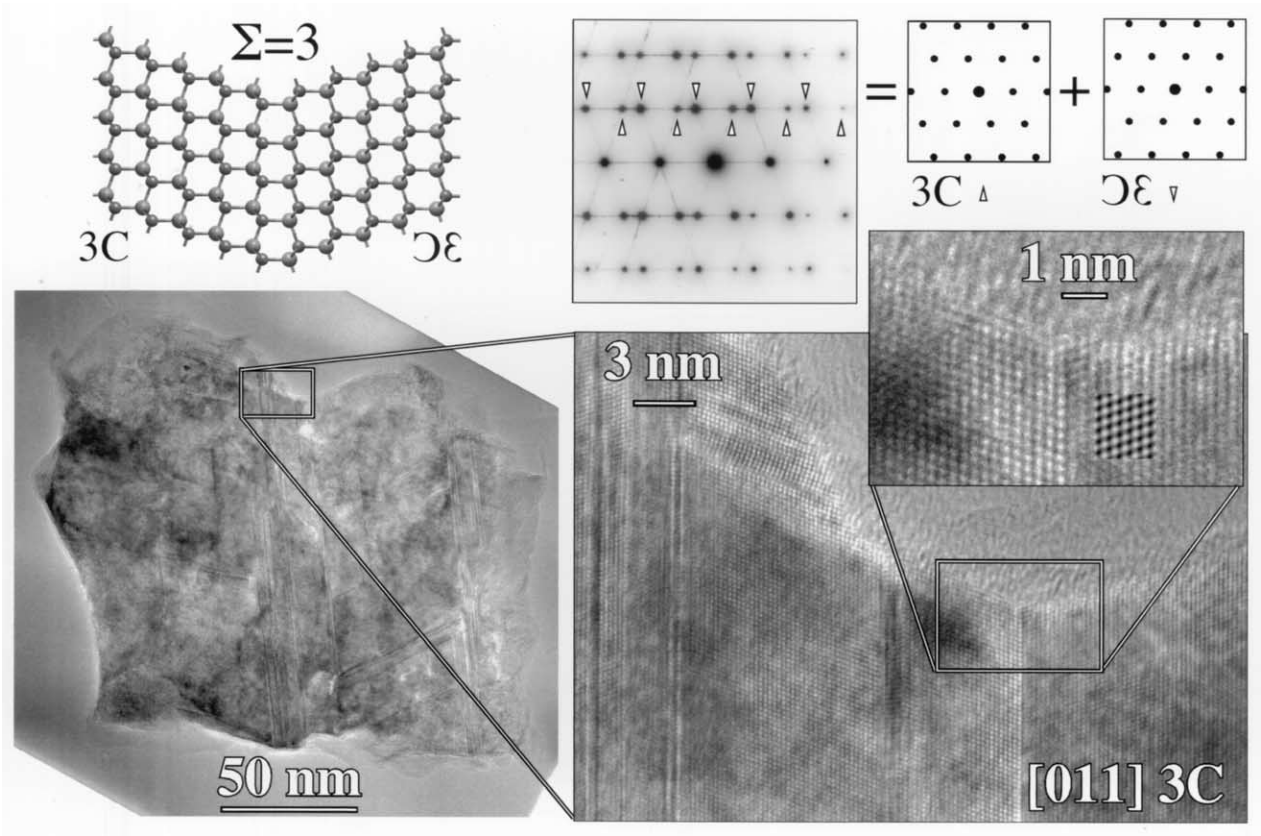

Fig. 5. A Σ=3 twinned, 3C β-SiC grain from Murchison KJB. A bright field image of the grain is shown along with progressively magnified high-resolution lattice images showing cross-lattice planes. Inset in one high-resolution image is a simulated lattice image which matches the defocus/thickness conditions of the micrograph. Random stacking faults along <111> directions are evident in the high-resolution images and from the streaking in corresponding <111> directions in the SAED pattern. An atomic model for the low-energy Σ=3 {111} twin interface is shown.

ture is described as a first order Σ=3 CSL (Ranganathan, 1966; Randle, 1993). The value of Σ represents the ratio of the areas of the unit cell (projected along a specified zone axis, in this work <011>) of the coincident lattice (defined by lattice points in coincidence between two twin-related lattices) to that of the untwinned unit cell. Twin components of a CSL are related by a rotation about the common crystallographic axis. For Σ=3, this rotation is $\theta = 70.53°$ about a <011> axis, and for SiC an additional rotation of 180° is required to establish C-Si bonds across the Σ=3 interface as opposed to C-C or Si-Si bonds. The most common twin structure in fcc crystals is the lowest order Σ=3, however, high order boundaries such as Σ=9 ($\theta = 38.94°$) or Σ=27 ($\theta = 31.59°$) can form perpendicular to {011} planes when multiply twinned Σ=3 related domains intercept, e.g., (Σ=3) x (Σ=3) -> (Σ=9). The twin boundaries observed in Murchison 3C SiC are almost entirely Σ=3.

In a cubic lattice, there are four sets of {111} planes available to form Σ=3 twin boundaries: two are oriented "edge-on" and two are "inclined" to any particular <011> zone axis. Only Σ=3 boundaries associated with edge-on {111} planes are visible along a <011> zone axis. For example, in [011] SAED patterns, Σ=3 twinning across $(11\bar{1})$ and $(1\bar{1}1)$ edge-on planes produce extra Bragg reflections, whereas no extra reflections arise from twinning across (111) or $(\bar{1}11)$ inclined planes (see Fig. 6). Each inclined-twin domain will have a <114> zone coincident with the [011] zone axis of the twin-related primary domain: $[\bar{4}11]$ for (111) inclined domains and $[4\bar{1}1]$ for $(\bar{1}11)$ inclined domains. Since <011> zones contain all the diffracted beams present in <114> zones, no extra reflections are created by the inclined-twin domains. Furthermore, no lattice fringes are visible from inclined Σ=3 twin domains because the projected lattice plane spacings along <114> are 1.31 Å-spaced $\{1\bar{1}3\}$ and 1.54 Å-spaced $\{02\bar{2}\}$ that are beyond the resolution of the TEM instrument used in this study. Nonetheless, the presence of inclined twin domains can be inferred by comparing dark field images formed by <114> zone axis reflections, such as $\{1\bar{1}3\}$, to dark field images using a reflection unique to <011> zones, such as {111}. However, considering the large number of grains analyzed, such an analysis would be time-prohibitive. Therefore, Σ=3 twin domains associated with inclined {111} planes were not detected in this work. This point has relevance for the determination of the polytype distribution as discussed in Section 3.2.

It is common to observe <011> SAED patterns from 3C β-SiC grains that exhibit extra reflections at positions 1/3{111} along one or both edge-on {111} plane normals. These reflections do not reflect a modification of the 3C unit cell as shown by Bender et al. (1986) for fcc Si; rather they arise from plural scattering produced by the presence of Σ=3 twin domains (Fig.

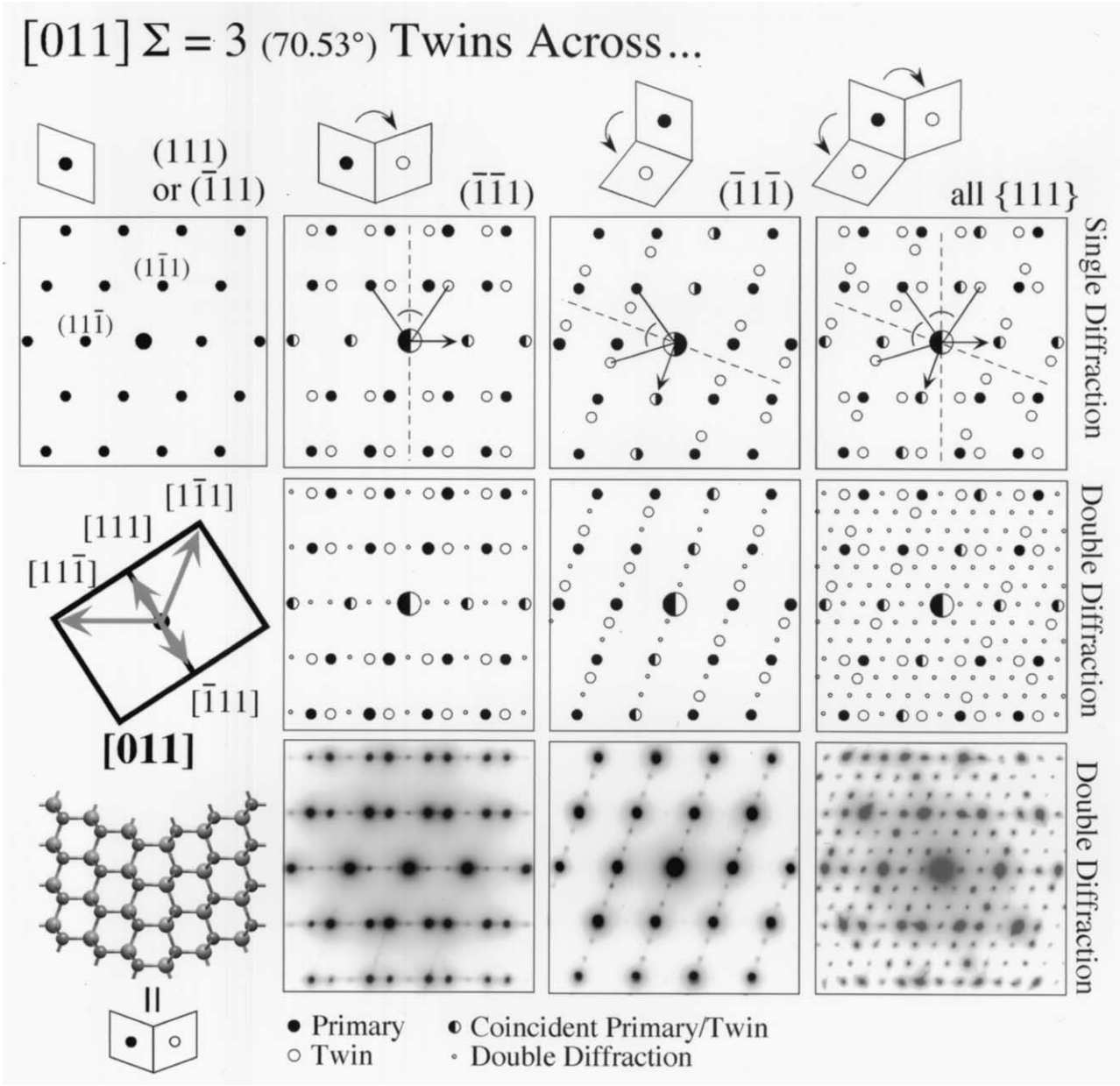

Fig. 6. Diffraction patterns along the [011] direction of 3C β-SiC with $\Sigma=3$ twinning along the four unique <111> directions. Crystallographic directions are illustrated by the unit cell. The components of a [011] $\Sigma=3$ CSL are related by relative rotation of the lattices by 70.53° (plus an additional 180° to form C-Si bonds) about [011]. This is shown schematically by the rhombi representing the 3C lattice; black circles primary domain, open circles twin domain. Schematic illustrations of calculated diffraction patterns with single diffraction (top row) and double diffraction (middle row) are shown. Primary reflections are black circles, twinned reflections are open circles, and coincidence reflections are black/white circles. The dashed lines and arrows illustrate the orthogonal mirror symmetry planes in the diffraction patterns. The arrow points to an *(hkl)* reflection corresponding to the mirror plane direction indicated above each pattern. The lines separated by an arc illustrate the relative rotation (minus 180°) between the twin related lattices. Representative examples of 3C β-SiC SAED patterns are shown (bottom row). In the example illustrating twinning across (111), twin reflections are as strong as the primary reflections. In the example of twinning across (1$\bar{1}$1), the twinned reflections are weaker than the primary reflections, but slightly more intense than the double diffraction spots, illustrating the range in relative intensities of primary, twinned, and double diffraction reflections.

6). A diffracted electron beam emerging from one twin domain can act as the principal beam for a second twin domain that diffracts the beam again. The 1/3{111} reflections occur along one direction if the twinning is predominantly across one set of edge-on planes and along both directions if major twinning is across both sets of edge-on planes (Fig. 6). The strength of the 1/3{111} reflections depends on the electron path length through the twin domains as well as the arrangement of the

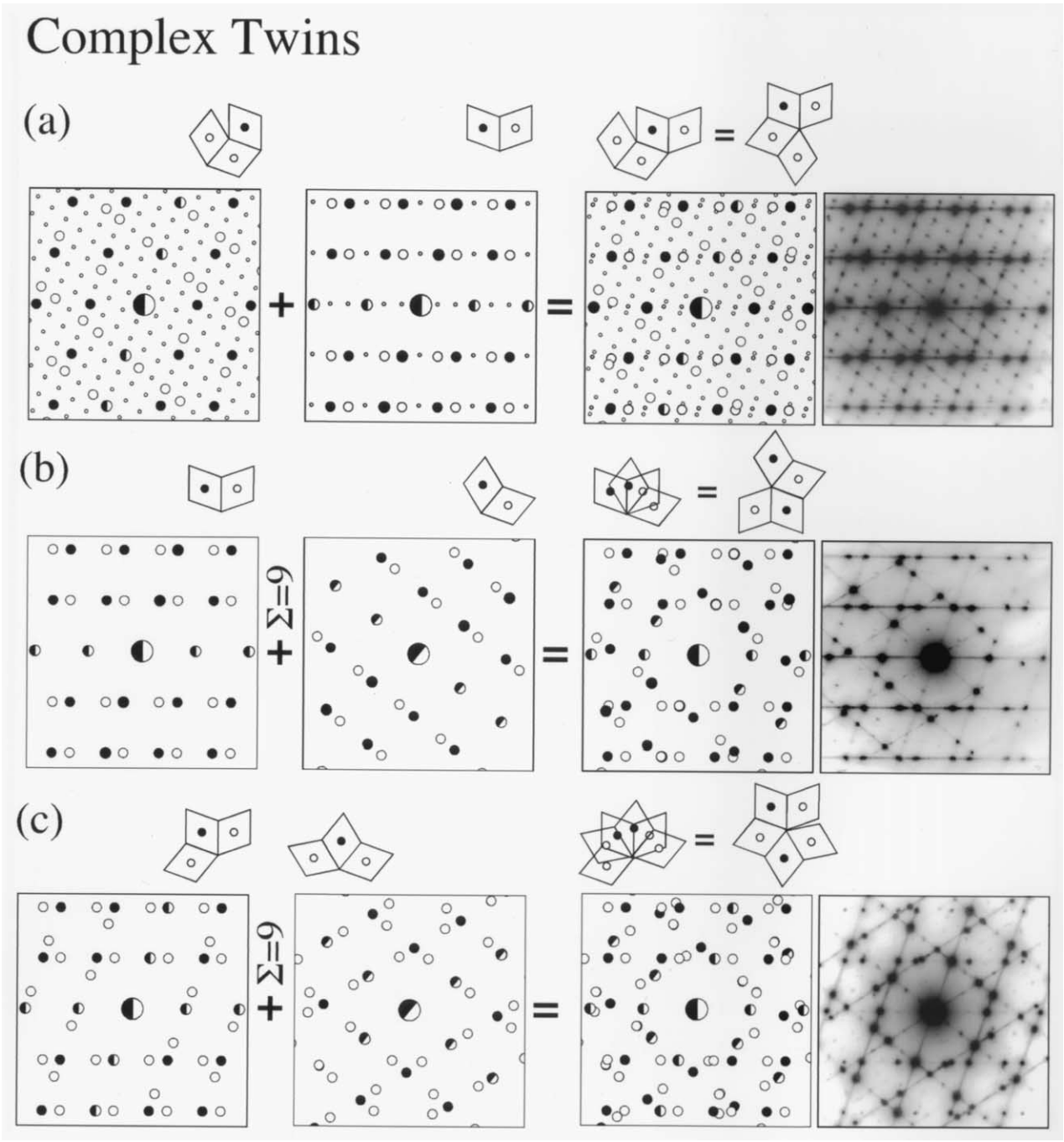

Fig. 7. Complex twin microstructures along the [011] direction in 3C β-SiC from Murchison KJB. Three examples of SiC grains are shown, each containing two domains with $\Sigma=3$ twin microstructure which (a) share a common domain orientation and (b, c) are related by a $\Sigma=9$ boundary. Schematic illustrations are shown of diffraction patterns from each of the two twin related domains (actual SAED patterns not shown). Symbol definitions are same as in Figure 6. Actual (entire grain) SAED patterns from each of the grains are shown at the far right.

domains. The 1/3{111} reflections are accompanied by an intensity modulation of every third {111} lattice fringe along the associated direction in corresponding HR-TEM lattice images (Bender et al., 1986).

Complex twin microstructures are present in presolar 3C β-SiC (Fig. 7). An example of multiple $\Sigma=3$ twinning in a SiC grain is shown in Figure 7a. The diffraction pattern from the whole grain contains two sets of double diffraction spots that reveal this grain has two large domains, each with its own $\Sigma=3$ twin structure, and sharing a common $\Sigma=3$ boundary. This is confirmed by SAED of each separate domain. Examples of mixed Σ-twin microstructures in SiC grains are shown in Figure 7b and Figure 7c, where SAED reveals that the grains have two domains containing $\Sigma=3$ twin microstructure that are

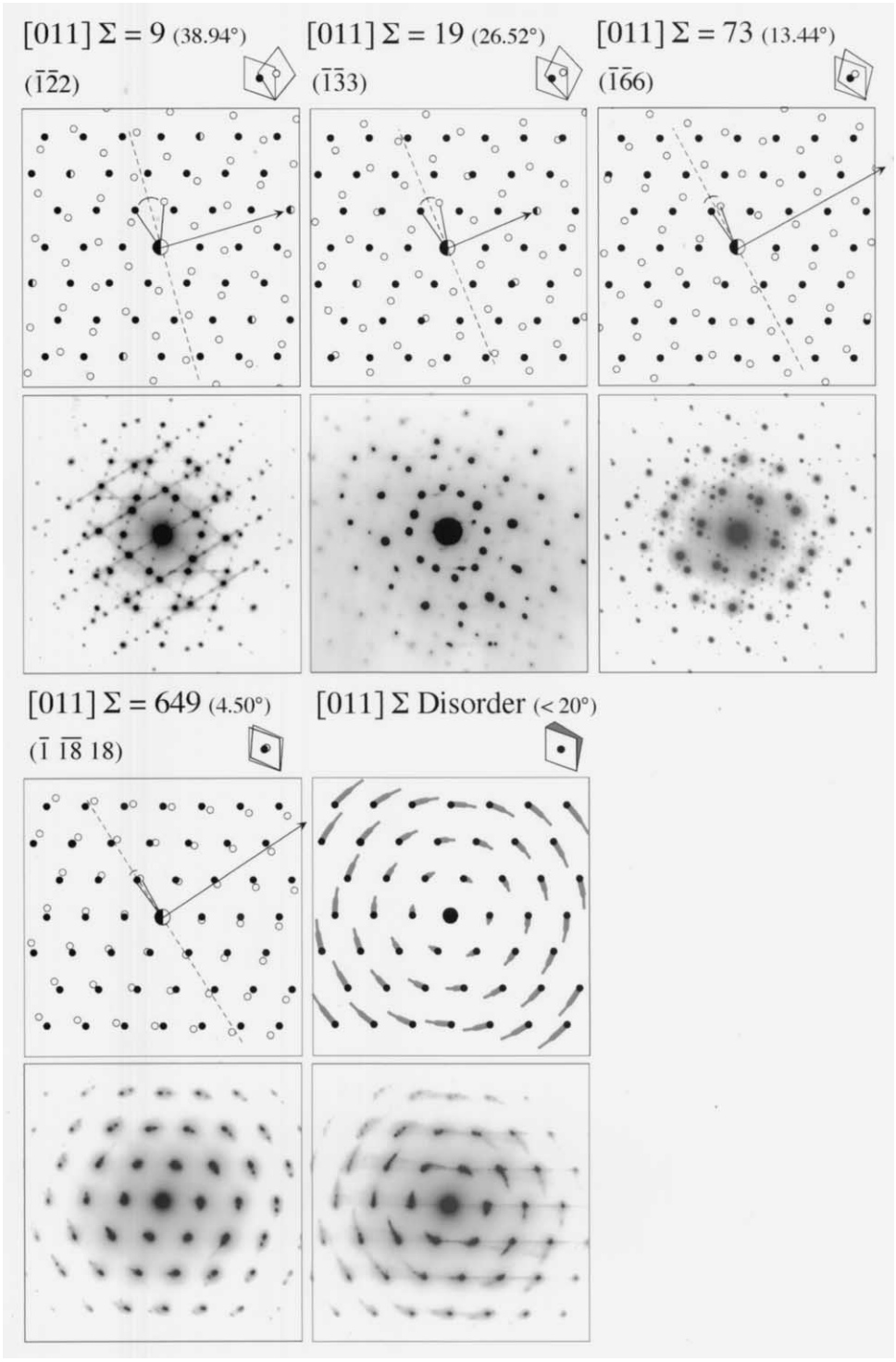

Fig. 8. High order Σ=9, Σ=19, Σ=73, Σ=649, and Σ-disordered twin microstructures along the [011] direction in 3C β-SiC from Murchison KJB. Symbol definitions are same as in Figure 6. The grain identified with a Σ=649 (θ = 4.499°) twin microstructure exhibited two sets of [011] zone axis reflections rotated with respect to one another by 4.51 ± 0.05°. The example of a low-angle boundary Σ-disordered 3C SiC grain shows the maximum disorder observed. Double diffraction is apparently present in some of the diffraction patterns.

related by a high order Σ=9 (38.94°) twin boundary. This is also confirmed by SAED of each domain. Additional high order twin boundaries observed in presolar SiC grains are Σ=19 (θ = 26.53°), Σ=73 (θ =13.44°), and Σ=649 (θ =4.50°) (Fig. 8). Grain boundaries having Σ= 9, 19, and 33 (θ = 20.05°) are usually observed in epitaxial CVD films where separate <011> oriented fcc grains growing on the substrate impinge (e.g., see Narayan et al., 1990; Dorignac et al., 1997). High

Table 1. [011] Coincidence Site Lattices up to $\Sigma=107$.

Σ	θ (°)	First Diffraction Twin Plane	Second Diffraction Twin Planes
3	70.529	{1 1 1}	{2 1 1}
9	38.942	{1 2 2}	{4 1 1}
11	50.479	{2 3 3}	{3 1 1}
17	86.628	{4 3 3}	{3 2 2}
19	26.525	{1 3 3}	{6 1 1}
27	31.586	{2 5 5}	{5 1 1}
33a	20.050	{1 4 4}	{8 1 1}
33b	58.992	{4 5 5}	{5 2 2}
41	55.877	{3 4 4}	{8 3 3}
43	80.631	{6 5 5}	{5 3 3}
51a	16.099	{1 5 5}	{10 1 1}
51b	22.844	{2 7 7}	{7 1 1}
57	82.946	{5 4 4}	{8 5 5}
59	45.980	{3 5 5}	{10 3 3}
67	62.439	{6 7 7}	{7 3 3}
73	13.443	{1 6 6}	{12 1 1}
81a	38.942	{1 2 2}	{4 1 1}
81b	77.885	{8 7 7}	{7 4 4}
83	17.860	{2 9 9}	{9 1 1}
89	34.893	{4 9 9}	{9 2 2}
97	61.018	{5 6 6}	{12 5 5}
99a	11.536	{1 7 7}	{14 1 1}
99b	89.421	{7 5 5}	{10 7 7}
107	33.718	{3 7 7}	{14 3 3}

order grain boundaries (see Table 1) have large interfacial energies and their formation is much less energetically favorable than $\Sigma=3$ boundaries. Evidence that high order grain boundaries with interface angles $< 20°$ are unstable is evident by the previously discussed rotational disorder about the <011> axis in the SAED patterns (Fig. 8) of $\approx 16.5\%$ of the 3C-SiC Murchison population (defined as single polytype 3C-SiC grains). This rotational disorder can be attributed to Σ disorder at a grain boundary in the form of a range of high order Σ boundaries (with small interface angles) that arise from the growth instabilities of the high energy boundaries.

Single crystals of 3C SiC, defined as grains with very faint to no visible twin reflections present in their diffraction patterns represented 66.4% of the 3C-SiC Murchison population, and approximately 10.7% of these single crystals exhibited Σ-disorder. Not all possible twin planes are visible along any one [011] zone axis, therefore this is only an upper limit for the fraction of 3C-SiC single crystals present. The fractions of all 3C-SiC Murchison grains exhibiting visible, well defined Σ-twin boundaries are approximately $\Sigma=3$ (32.6%), $\Sigma=9$ (0.91%), $\Sigma=19$ (0.23%), $\Sigma=73$ (0.23%), and $\Sigma=649$ (0.23%).

A recent study of a pristine (i.e., not isolated by acid dissolution) 3C-SiC grain from the Cold Bokkeveld (CM2) carbonaceous chondrite reported evidence for randomly oriented graphite included in the grain (Stroud et al., 2002). In that work, the SAED pattern of the $\Sigma=3$ twinned SiC exhibited superimposed diffraction rings that indexed to graphite: 0.342 nm (002) and 0.212 nm (100). No similar diffraction rings were observed in the over 508 individual KJB SiC grains examined here. In addition, no sets of non-SiC reflections (e.g., from internal subgrains) were identified in any of the KJB SiC grains studied (although detailed examination was restricted to only one zone axis, i.e., 3C <011> and 2H <11$\bar{2}$0>).

3.1.2. Microstructure of presolar 2H/3C intergrowth SiC

Figure 9 shows an example of a Murchison KJB SiC grain whose electron diffraction pattern has a set of extra reflections that are inconsistent with 3C SiC twin reflections or double diffraction. The extra reflections are most evident along the horizontal row of Bragg reflections that intersect the primary beam, (000). If the reflections arose from 3C $\Sigma=3$ double diffraction, there should be two equally spaced 1/3{111} reflections between (000) and the primary {111} peak, as opposed to the one diffraction spot actually present. This set of extra Bragg peaks is consistent with reflections along the <11$\bar{2}$0> zone of a domain of 2H α-SiC. In fact, diffraction patterns from separate 2H and 3C SiC domains could be isolated using the smallest SAED aperture (Fig. 9), further demonstrating this grain is an intergrowth of two SiC polytypes. The streaking in the 2H diffraction pattern indicates the presence of stacking faults along the [0001] direction. As expected, the bright-field (BF) images of the intergrowth grain show stacking faults in the 2H domain along the [0001] tetrahedral stacking direction. However, HR-TEM shows that long-range 2H order is also present (Fig. 9). The diffraction pattern of the 3C domain contains diffuse streaking of lesser intensity along several (111) directions, indicating a lower density of stacking faults, consistent with the BF image. Two thirds of this intergrowth grain is in the form of 2H SiC.

The proportion of 2H to 3C order in different SiC intergrowth grains varied from predominantly 2H to predominantly 3C. The 3C domains of the intergrowth grains displayed a range of $\Sigma=3$ twin microstructures and stacking fault densities. Stacking faults are observed in 2H domains, but no twinning is observed. Although each 3C domain in an intergrowth grain has four sets of cubic <111> directions that can serve as an homoepitaxial growth interface to a 2H domain, in almost all intergrowth grains there was a single dominant 2H-domain orientation. In those cases, either a single 2H domain or parallel, alternating 2H and 3C lamellae were observed. In comparison, only one intergrowth grain was observed to have two different prevailing 2H-domain orientations.

It is important to note that only those 2H domains associated with edge-on 3C {111} planes will produce phase contrast lattice fringes and clearly recognizable SAED reflections. The 2H domains associated with inclined 3C {111} planes will not have any hexagonal high symmetry zone axis in coincidence with the imaged 3C [011] axis; the closest hexagonal low index zone, <10$\bar{1}$1>, is separated by $\approx 11.5°$ from the imaged 3C [011]. Consequently, inclined 2H domains are hard to detect because they do not produce phase contrast lattice fringes and produce only weak diffraction patterns. This point has relevance for the determination of polytype distributions as discussed in Section 3.2.

3.1.3. Microstructure of presolar 2H α-SiC

An example of a single crystal 2H α-SiC grain is shown in Figure 10. Diffuse striations in the [11$\bar{2}$0] SAED pattern along the [0001] direction indicate the presence of a moderate number of stacking faults. High-resolution lattice images show that long-range 2H order is present in the grain (Fig. 10). There is no analog in 2H SiC of a 3C $\Sigma=3$ twin boundary, (e.g.,

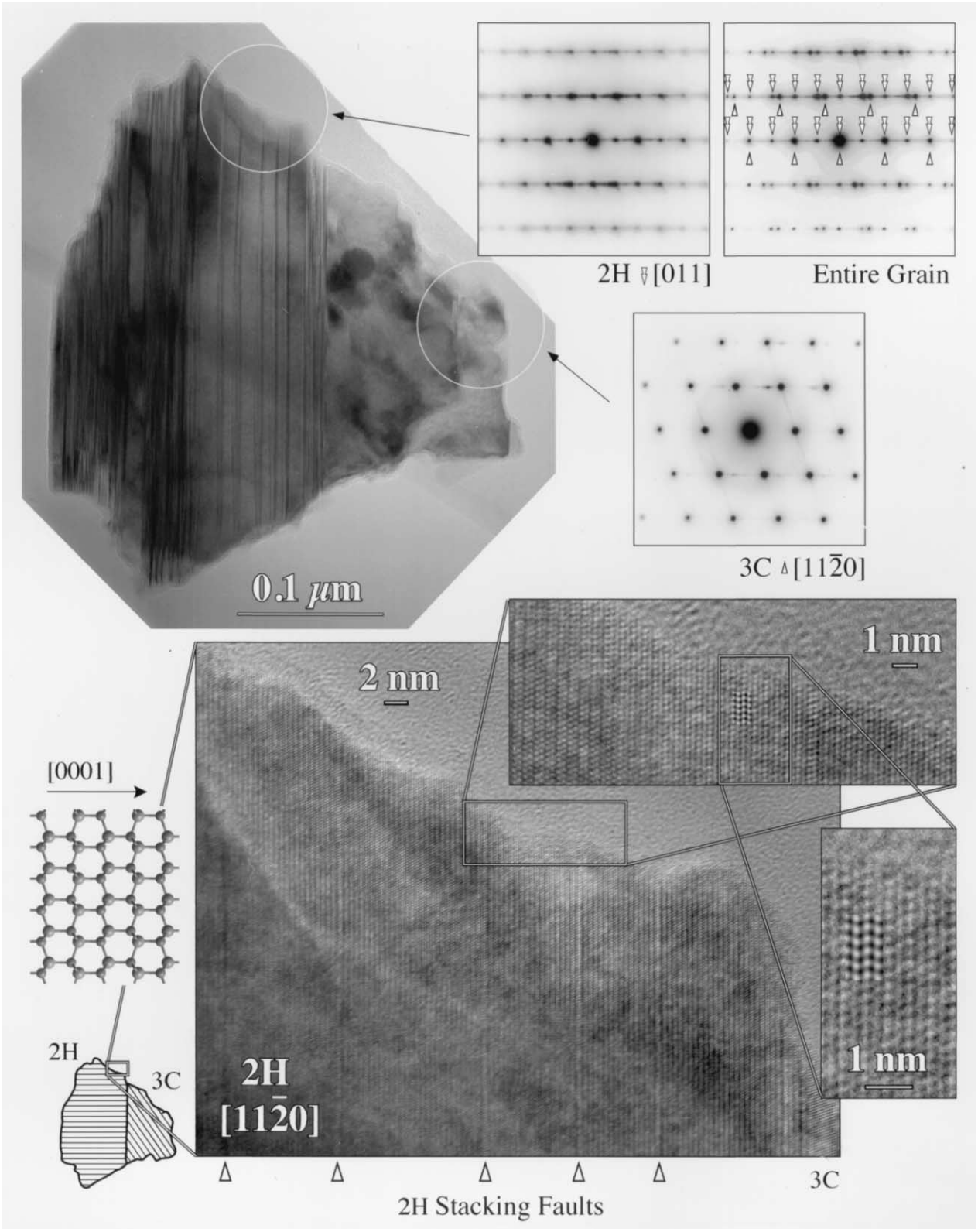

Fig. 9. Intergrowth SiC grain containing predominantly 2H with one 3C growth domain from Murchison KJB. The SAED pattern from the entire grain is a composite of diffraction patterns from the 2H [11$\bar{2}$0] and 3C [011] oriented SiC domains. A bright field image of the grain is shown along with progressively magnified high-resolution lattice images showing cross-lattice planes. Inset in the high-resolution image is a simulated lattice image calculated under defocus/thickness conditions which match the lattice fringes in the micrograph. Long-range 2H order is evident in the lattice images of the 2H SiC domain.

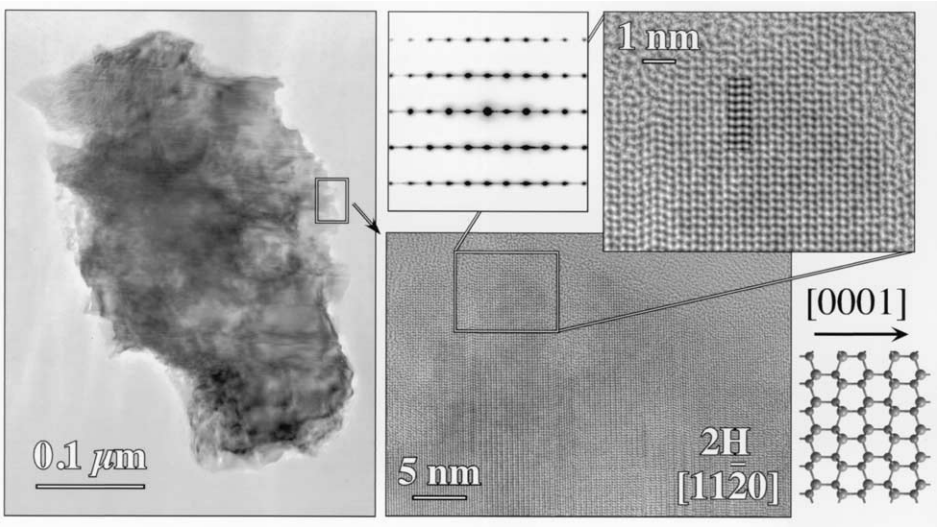

Fig. 10. A single crystal 2H α-SiC grain from Murchison KJB. The SAED pattern from the entire grain indexes to the [11$\bar{2}$0] zone of 2H SiC. A bright field image of the grain is shown along with progressively magnified high-resolution lattice images showing cross-lattice planes. Inset in the high-resolution image is a simulated lattice image calculated under defocus/thickness conditions which match the lattice fringes in the micrograph.

twinning across tetrahedral {0001} planes) because such a 2H twin domain would be identical to the original lattice. For twinning to occur in 2H SiC, a high-energy twin interface must form instead. Since lower energy structures, such as stacking faults, can more readily form to relieve strain, the formation of a 2H-twin interface is energetically unfavorable in comparison with stacking fault formation. It is thus not surprising that electron diffraction and HR-TEM show no evidence of twinning in 2H SiC grains and that, within the same 2H/3C intergrowth grain (see Fig. 9), higher densities of stacking faults are observed in the 2H domains than in the 3C domains.

One 2H α-SiC grain in Murchison contained two α-SiC domains sharing common [11$\bar{2}$0] zone axes that were misoriented by 2.4°. The smaller of two domains contained a high density of stacking faults and was disordered. Another 2H α-SiC grain in Murchison appeared in bright field imaging to be three discrete grains in a cluster, however these were in fact slightly misoriented domains of a single 2H α-SiC grain. The three domains shared common [11$\bar{2}$0] zone axes misoriented by 3.0°, 2.4°, and 2.2° from one another, also the domains were rotated by several degrees about their [11$\bar{2}$0] axes. Some 3C β-SiC grains exhibited a similar microstructure consisting of several 3C domains sharing common [011] axes that were misaligned by small angles.

3.1.4. Microstructure of presolar one-dimensionally disordered SiC

An example of a SiC grain in which the tetrahedral stacking is heavily disordered is shown in Figure 11. The SAED diffraction pattern shows heavy streaking along one crystallographic direction, corresponding to a high density of stacking faults. The BF image of the grain shows numerous parallel striations. Both SAED and HR-TEM lattice images show no clear evidence of any dominant polytype order. Only short-range order (over several unit cells) of different polytypes was observed by HR-TEM. The density of stacking faults in these grains is so high that their structure is best described as randomly stacked, tetrahedral close-packed sheets, and therefore they cannot be classified as any polytype structure.

3.1.5. Higher order polytypes of presolar SiC

Several percent of the SiC grains examined in Murchison KJB did exhibit a few very weak diffraction spots in their SAED patterns suggesting either 4H or 6H order. However these SAED patterns also contained diffuse striations (e.g., stacking faults), and double diffraction spots. Furthermore, HR-TEM lattice images did not show evidence of 4H or 6H order that repeated more than several unit cells in any of SiC grains examined. Therefore, no conclusive evidence for small domains of 4H or 6H order was found, other than what could be expected from random stacking faults.

3.2. Abundance Distribution of Presolar SiC Polytypes

There are difficulties inherent in determining relative abundances of grain types using SAED patterns and HR-TEM images from a limited set of crystallographic directions (as in this work where one direction was examined). Difficulties arise because of finite tilt range of the TEM goniometer and the fact only two-dimensional crystallographic information is contained in SAED and HR-TEM data. Because of the finite tilt limits of the goniometer, a fraction of the randomly oriented grains will have no suitable high symmetry zone axes accessible for polytype identification. This fraction varies among SiC polytypes with distinctly different crystallographic symmetries (i.e., cubic, hexagonal, and rhombohedral). For example, there are six coplanar $<11\bar{2}0>$ hexagonal directions lying in the (0001) plane compared to twelve $<011>$ cubic directions isometrically distributed in three dimensions. Consequently, the fraction of grains that can be identified varies with crystal system,

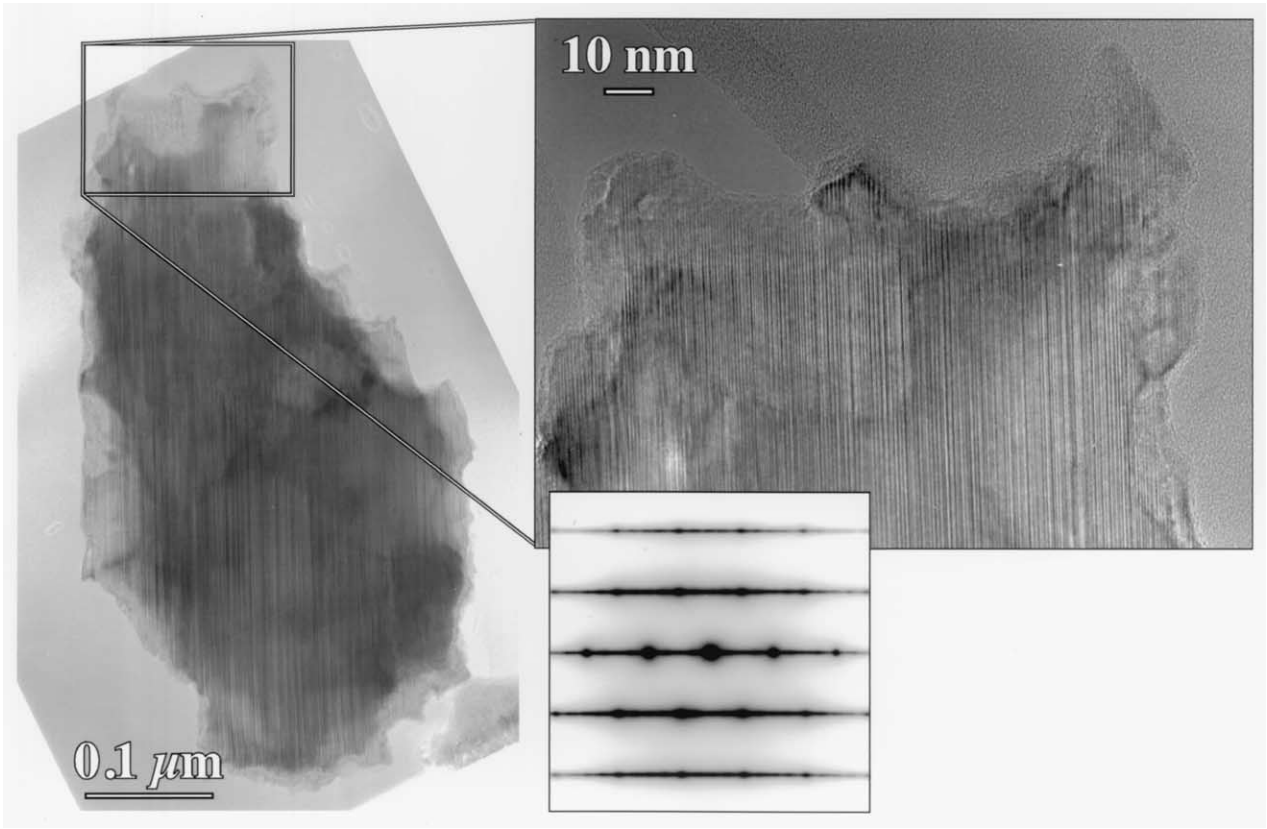

Fig. 11. One-dimensionally disordered SiC grain from Murchison KJB. The SAED pattern has intense streaking along the tetrahedral sheet stacking direction indicating a high density of stacking faults, as confirmed by the bright-field and HR-TEM lattice images.

biasing TEM measured polytype distributions. Nonetheless, the true distribution can be estimated from TEM measurements with appropriate corrections applied.

The relationship between the actual number of grains, N, of a particular polytype, and the number N_T identified by TEM can be described as

$$N = N_T (\varepsilon_i \varepsilon_o)^{-1} \quad (1)$$

where ε_i is the intrinsic fraction of randomly oriented crystals that have at least one zone axis perpendicular to the tetrahedral stacking direction (e.g., cubic <011> and hexagonal $<11\bar{2}0>$) within the TEM goniometer tilt limits. The parameter ε_o represents an observer bias arising from the relative difficulty in tilting a polytype perpendicular to the tetrahedral stacking direction and is difficult to quantify. When possible, grains were tilted until identified, in order that ε_o approached unity. In practice, $\varepsilon_o{}^{2H} < \varepsilon_o{}^{3C}$, meaning ε-corrected abundances with ε_o assumed 1 (as here) are underestimations of the actual 2H SiC population. Over 90% of the grains examined in the TEM were successfully identified. Most of the unidentified grains were revealed upon tilting to be part of a random cluster of grains, and consequently were not examined further.

The parameter ε_i was calculated for goniometer tilt limits of $\pm$ 45° and $\pm$ 30° (solid angle $4\pi \times 0.1179$) using an advanced version of the software package Sphere (Daulton, 1992). Relevant crystallographic zone axes of a polytype(s)/twin-structure configuration were mapped onto the surface of a unit sphere. The relevant zones were <011> for 3C SiC, $<11\bar{2}0>$ for 2H SiC, and 3C <011> zones coincident with 2H $<11\bar{2}0>$ for 2H/3C SiC intergrowths. Random grain orientations were modeled by rotating the mapped sphere using a spherically symmetric probability distribution. The fraction of random grain orientations that had at least one relevant zone axis within the goniometer tilt range defined in a fixed coordinate system were determined. The results of the calculations are given in Table 2 and the errors represent the standard statistical error of ten replicate calculations of 10^7 random grains.

In addition to crystal symmetry, ε_i is highly dependent on twin and polytype-intergrowth microstructure. This is because the presence of Σ-twin boundaries in a 3C SiC grain increases the number of unique <011> orientations. Furthermore, each 3C-twin domain has four sets of cubic <111> directions and each can serve as a growth interface to differently oriented 2H domains. The greater the number of uniquely oriented 2H domains, the greater the number of unique $<11\bar{2}0>$ orientations. Unfortunately, there is uncertainty in determining the actual grain microstructure because not all 3C $\Sigma=3$ twin planes are visible, e.g., the inclined twin planes. In addition, in 2H/3C intergrowth grains, only those 2H domains associated with edge-on 3C {111} planes will be visible. The correction factors in Table 2 assume that the only domains present are the visible ones. If invisible 3C-twin domains or 2H domains were

Table 2. Correction factors for Polytype Distribution Measurement Corresponding to TEM Goniometer Tilt Range of ± 45 and ±30.

Polytype	Microstructure[†‡]	Unique Directions	ε_i
2H		6 <11$\bar{2}$0>	0.60243 ± 0.00019
3C	0 × Σ=3	12 <011>	0.98590 ± 0.00139
3C	1 × Σ=3	18 <011>	0.99808 ± 0.00037
3C	2 × Σ=3	24 <011>	0.99988 ± 0.00003
3C	>3 × Σ=3	>24 <011>	≈1
3C	1 × Σ=9	22 <011>	0.99922 ± 0.00017
3C	1 × Σ=19	22 <011>	0.99948 ± 0.00004
3C	1 × Σ=73	22 <011>	0.99988 ± 0.00003
3C	1 × Σ=649	22 <011>	0.99731 ± 0.00004
3C/2H	0 × Σ=3 1 × 2H	6 <011>/<11$\bar{2}$0>	0.60243 ± 0.00019
3C/2H	0 × Σ=3 2 × 2H	10 <011>/<11$\bar{2}$0>	0.88858 ± 0.00222
3C/2H	0 × Σ=3 >2 × 2H	12 <011>/<11$\bar{2}$0>	0.98590 ± 0.00139

[†] $n \times \Sigma = b$ indicates the number, n, of unique 3C twin boundaries of order b.
[‡] $n \times$ 2H indicates the number, n, of unique 2H domains.

present, the actual ε_i correction factor for the grain would be higher than those in Table 2 with the maximum possible value of ε_i of 1. This uncertainty in ε_i for each grain is propagated into the errors of the polytype distribution. The ε-corrected relative polytype abundances are displayed in Table 3, which summarizes the principal experimental results of the present work. These results demonstrate that the KJB residue contains a large number of SiC grains with 2H structure ($19.78^{+0.39}_{-5.77}$%) as both intergrowths and single crystals, in addition to the dominant cubic 3C grains.

As noted in the Introduction, Virag et al. (1992) found that among the very large Murchison L-series SiC grains (1.5–26 μm), only the cubic 3C grains were isotopically anomalous (presolar), and that all α-SiC grains measured had normal isotopic compositions. However, in KJB, which is representative of the majority of presolar SiC grains in Murchison, >99% of the SiC grains were found to be isotopically anomalous, hence presolar (see Sect. 2.1.1). This observation, coupled with the large abundance of 2H SiC grains in KJB, as described above, leads us to conclude that *2H must also be a presolar SiC polytype*. Indeed, from the analysis of 508 grains, 2H appears to be the *only* non-cubic polytype of presolar SiC. Moreover, no 4H, 6H, 15R, or higher SiC polytypes were observed, essentially ruling out the possibility of terrestrial SiC contaminants in KJB (see Sect. 2.2.3).

Table 3. Murchison KJB SiC Polytype Distribution.[a]

Grain Type	Population[b] (% by number)	
3C	$79.35^{+6.66}_{-0.20}$	
2H/3C Intergrowths	$17.08^{+0.32}_{-5.70}$	$19.78^{+0.39}_{-5.77}$
2H	$2.70^{+0.22}_{-0.91}$	
Disordered	$0.89^{+0.20}_{-0.20}$	
All other polytypes	< 0.20	

[a] Based on TEM characterization of 508 grains, corresponding to > 90% of the total grains examined. Those excluded are grains that upon tilting were found to be actually two grains randomly stuck together, grains with no suitable zone axes within the goniometer tilt limits, and grains that became obstructed by the TEM Cu grid bar, at high tilt angle, before a suitable zone axes was reached.
[b] ε_i corrected, assuming $\varepsilon_o = 1$.

3.3. Isotopic composition of a 2H α-SiC Murchison Grain

To definitively establish the presolar origin of 2H α-SiC grains isolated from Murchison, we performed an isotopic analysis of a TEM-characterized 2H SiC grain (Fig. 12) from the KJE separate using NanoSIMS. The grain is 5.1 μm long with a serrated perimeter and a needle-like morphology. The long dimension of the needle is rotated in the (11$\bar{2}$0) plane by ≈ 43° from the [0001] crystallographic direction. Although the needle-like morphology is not uncommon, most presolar SiC grains are roughly equant in aspect ratio. Isotopic-composition maps of $^{12}C/^{13}C$ and $^{14}N/^{15}N$ for the grain are shown in Figure 13. The grain is clearly isotopically anomalous as shown by the differences in isotopic composition between the terrestrial a-C support film and the grain. The mean C isotopic composition of the grain is $^{12}C/^{13}C = 64 \pm 4$ (terrestrial =89), and the mean N isotopic composition is $^{14}N/^{15}N = 575 \pm 24$ (terrestrial = 272), both within the range of mainstream presolar SiC. These isotopic results reaffirm our conclusion that 2H is also a presolar SiC polytype.

4. DISCUSSION

4.1. Presolar SiC Polytypes: Condensates or Thermal Transformation Products?

We propose that the SiC polytype distribution in Murchison KJB reflects original growth abundances as opposed to post-growth thermal transformation in the solar nebula. Appreciable transformation of 2H SiC ->3C SiC and 3C SiC ->6H SiC require at least 1673–1773 K and 1973 K, respectively (Krishna

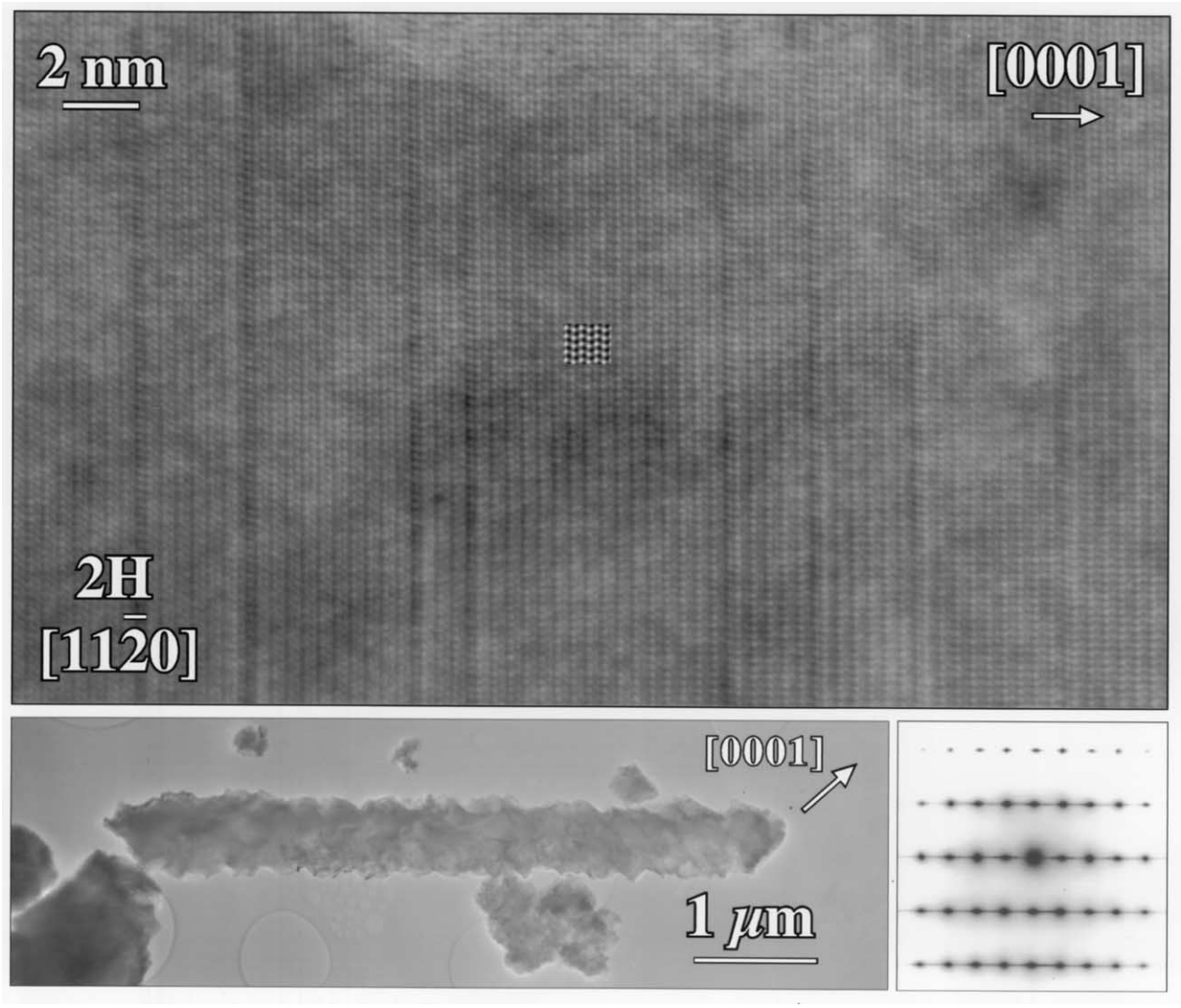

Fig. 12. Circumstellar 2H α-SiC crystal from Murchison KJE. Its presolar origin is confirmed by NanoSIMS isotopic analysis (cf. Fig. 13). This SiC crystal has a needle-like morphology with a serrated perimeter. Although this grain morphology is not uncommon, most SiC in Murchison have a roughly unit (equant) aspect ratio.

et al., 1971; Krishna and Marshall, 1971a; Bootsma et al., 1971). In comparison, experimental studies of volatization kinetics predict that SiC grains (diameter $\leq$1 μm) would be destroyed by reducing nebular gases $\geq$1173 K in less than several thousand years (Mendybaev et al., 2002). Furthermore, the P3 presolar noble gas abundances in CV3 meteorites imply that the constituents of the meteorite, before and following accretion, experienced peak temperatures $<$870 K (Huss, 1997). Murchison has a lower metamorphic grade (CM2), so its constituents experienced still lower temperatures. Although 6H SiC can also form directly by condensation, the fact that we identified no intergrowths or single crystals of the 6H polytype in presolar SiC supports the proposition that the population does not contain thermal transformation products. If 6H SiC (or higher order polytypes) were present, sampling statistics constrain their abundance to be $<$0.2% (Table 3). Therefore, only a very small fraction of the population, at most, could be thermal transformation products.

4.2. Stellar Sources of Presolar SiC

Isotopic studies of individual SiC grains isolated from meteorites show that they fall within several distinct presolar populations. The majority of presolar SiC grains ($\sim$94%), designated "mainstream" (Hoppe et al., 1994b), have individual grain isotope compositions characterized by AGB star *s*-process isotopic signatures in one or several of the following elements: Kr, Sr, Zr, Mo, Xe, Ba, Nd, Sm, and Dy (see Zinner et al., 1991b; Prombo et al., 1993; Lewis et al., 1994; Hoppe and Ott, 1997; Nicolussi et al., 1997, 1998; Podosek et al., 2002). Furthermore, the distribution of $^{12}C/^{13}C$ ratios (between 10–100) in mainstream grains is similar to that of carbon star envelopes (Anders and Zinner, 1993; Alexander, 1993). Silicon and Ti isotopic compositions in mainstream SiC grains are a result of the combined contributions from both the initial compositions of the parent AGB stars and nucleosynthesis in the He-shell of these stars. The variations in the initial composi-

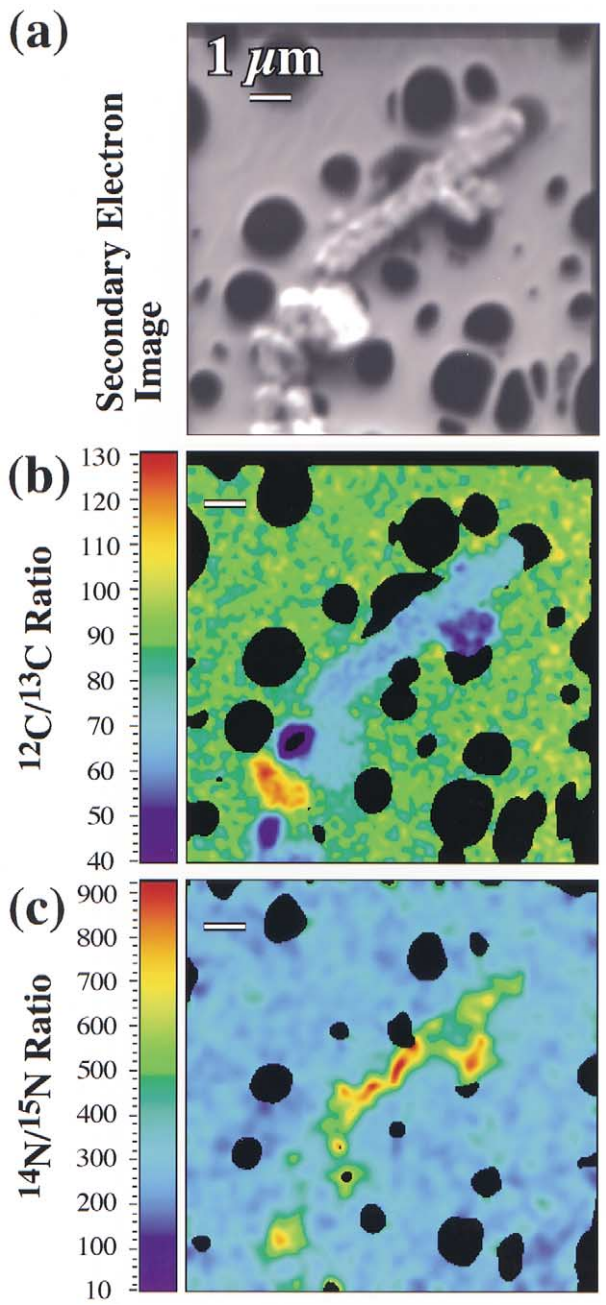

Fig. 13. NanoSIMS (a) secondary electron image as well as isotopic ratio maps of (b) $^{12}C/^{13}C$ and (c) $^{14}N/^{15}N$ for the circumstellar 2H α-SiC shown in Figure 12. The C and N isotopic ratios of the grain are clearly different than the terrestrial ratios in the background supporting holey carbon film, proving its presolar origin as circumstellar dust. The C and N isotopic ratios are typical of mainstream presolar SiC (see text for discussion).

tions of AGB stars can be explained by galactic chemical evolution (Timmes and Clayton, 1996; Clayton, 1997) and/or heterogeneities in the ISM (Lugaro et al., 1999).

Although their definitions vary slightly in the literature, four minor SiC subpopulations have also been classified: X, Y, Z, and A+B. Type X (~1% of total population) have relatively large inferred $^{26}Al/^{27}Al$ ratios, and are defined as having excesses in ^{28}Si (deficits in ^{29}Si and/or ^{30}Si) (Amari et al., 1992). Some X grains contain ^{44}Ca daughters of the short-lived ^{44}Ti (Amari et al., 1992; Hoppe et al., 1996b) that are only produced by explosive nucleosynthesis in supernovae (see Woosley and Weaver, 1995). Type Y (~1%) are defined by $^{12}C/^{13}C > 100$ and $^{14}N/^{15}N > 272$ (solar) (Amari et al., 2001a; Hoppe et al., 1994b). Type Z (~1%) are defined by $^{12}C/^{13}C < 120$ and large excesses of ^{30}Si relative to ^{29}Si (Alexander, 1993; Hoppe et al., 1997). Type Y and Z grains are believed to form around AGB stars with lower-than-solar metallicities (Zinner et al., 2001b). Type A+B grains (≈ 3–4%) are characterized by their low $^{12}C/^{13}C$ ratios (<10), a wide range of $^{14}N/^{15}N$ ratios (40–10000), and a Si isotopic distribution that is very similar to that of mainstream grains (Hoppe et al., 1994b; Amari et al., 2001b). Both J-type carbon stars and CH stars have been proposed as their sources (Lodders and Fegley, 1998).

We assume that the SiC in Murchison is a representative sample of SiC from all kinds of astronomical sources. Given that 95–96% of the SiC grains in Murchison come from carbon AGB stars (99% if possible small contributions from J-stars and/or CH stars is included), then *to first order the distribution of polytypes of presolar SiC from Murchison can be taken as the mean distribution in all circumstellar environments.*

The contribution of supernovae (~1%) to the SiC population is too small to account for the observed abundance of 2H SiC grains, and we thus conclude that *both* 3C and 2H SiC polytypes must form in the circumstellar outflows from AGB stars. In principle, supernovae contributions could account entirely for the small subpopulation of one-dimensionally disordered grains (<0.9%; Table 3), but without isotopic information on these grains it is currently impossible to evaluate this possibility. Nonetheless, future TEM microstructural studies of a sufficiently large number (several tens) of isolated X-grains, identified as such by SIMS ion imaging, could provide a definitive answer to the question of the crystal structure of SiC formed in supernova outflows.

4.3. SiC Polytype Growth and Circumstellar Condensation

As argued above, the majority (>95%) of presolar SiC is of AGB star origin. Since the range of isotopic compositions found in these grains suggest that many AGB sources with a range of metallicities contributed dust to the solar nebula (Gallino et al., 1994; Alexander, 1993; Lugaro et al., 1999), at best only general inferences on formation conditions can be extracted from the grain microstructures. Nevertheless, although physical parameters such as temperature gradients, pressure gradients, gas species, elemental abundances, irradiation fluences, etc. vary among AGB stars, the physical environments of SiC grain condensation should be restricted to a limited range of conditions. For this reason, it is justified to use microstructures of circumstellar SiC to deduce general information about grain forming regions.

There is not yet a detailed understanding of the parameters that affect SiC polytype formation, although many theories have been proposed (see Tairov and Tsvetkov, 1982; Matsunami, 1993; Fissel, 2000). No conclusive theory has emerged, and it remains enigmatic why under certain growth conditions only one particular polytype forms. Although many factors

such as source gas (Si/C ratio, molecular species, and pressure) and nature of growth surface can influence polytype growth, it is clear that temperature and kinetics play an important role. Since atmospheres of carbon stars are heterogeneous with many factors not well constrained, we decided to focus on temperature for a first order model of grain condensation.

A range of formation temperatures is reported in the literature for the most common SiC polytypes. However, it is not straightforward to deduce something akin to a phase diagram of SiC polytype formation from these studies because different processes are used to synthesize SiC and, for a particular process, many experimental parameters vary among investigations. Therefore, the temperature dependent diagram of SiC polytype formation reported by Knippenberg (1963), although alluring, is of limited use. The most pertinent data are found in studies that examine the relative temperature dependence of several polytypes synthesized by a given process in which only a few experimental parameters are varied. From such studies, general trends in the temperature dependence of SiC polytype formation are inferred and used here to interpret circumstellar SiC microstructures.

The 2H polytype of SiC is considered to be the lowest temperature polytype and was first synthesized by condensation on 1773 K graphite surfaces exposed to pyrolytically decomposed methyltricholorosilane (CH_3SiCl_3) gas (Merz and Adamsky, 1959). Others using this technique reported that 2H SiC formed between 1573–1723 K and was surrounded by regions of 3C SiC (Patrick et al., 1966; Powell, 1969; Berman and Ryan, 1971; Addamiano, 1982; Vetter et al., 2001). Furthermore, Patrick et al. (1966) reported almost entirely 3C SiC formed above 1700 K, consistent with the reported 2H ->3C SiC transformation temperature of 1773 K (Krishna et al., 1971; Bootsma et al., 1971). Although 3C can form above 2000 K, having a wide range of condensation temperatures, 3C is the only SiC polytype reported to grow near 2H SiC growth regions at low condensation temperatures. The 2H SiC polytype has also been synthesized by low pressure (1.3×10^{-3} dynes/cm^2) vapor condensation on slightly off-axis [0001] 6H-SiC substrates at 1473 K from pulsed laser ablated 3C SiC (Stan et al., 1994).

For any given vapor condensation process in which temperature is the major parameter varied, all polytypes other than 2H and 3C have formation temperatures greater than that of 3C SiC, however, under certain conditions their condensation temperature can be suppressed. For example, MBE deposition of 3C SiC occurs between 1273–1573 K while 6H SiC deposition occurs >1623 K on slightly off-axis [0001] 6H-SiC substrates from the decomposition of SiH_4, C_2H_4 and H_2 mixed gases (Kern et al., 1998). However, only 3C SiC grew on on-axis oriented substrates regardless of growth conditions (Kern et al., 1998). Polytype growth by vapor deposition is highly dependent on the material, orientation, preparation, and polarity (C-faced or Si-faced surface) of the substrate (see Matsunami, 1993; Tairov and Tsvetkov, 1982). In fact, surface steps produced by preparation of 6H substrates are used to suppress 3C SiC nucleation on terraces at low temperatures to promote 6H SiC growth; this technique is called step-flow or step-controlled epitaxy (Matsunami, 1993).

In CVD studies of growth on slightly off-axis [0001] 6H-SiC substrates at 10^6 dynes/cm^2 using SiH_3, C_3H_8 and H_2 gases, 3C SiC grew at 1373 K and 6H SiC grew between 1373–1773 K (Kimoto et al., 1993). In CVD studies using single-source organosilane precursor silacylobutane (c-$C_3H_6SiH_2$) at 6.7×10^3 dynes/cm^2, exclusively 3C SiC formed on [0001] oriented 6H-SiC substrates between 1073–1273 K and a mixture of 3C, 4H and 6H SiC formed at 1373 K (Yuan et al., 1995). Using sublimation-condensation (modified Lely process) on [001] oriented 3C-SiC substrates at 10^6 dynes/cm^2, 3C SiC is reported to form up to 2423 K while 6H (and some 15R) SiC formed above 2373 K (Yoo and Matsunami, 1991). In comparison, the transformation of the 3C-SiC substrate to 6H SiC was observed at 2523 K (Yoo and Matsunami, 1991). In another sublimation growth study, the deposition of predominantly 4H SiC was reported at 2473 K at 1.3×10^4 dynes/cm^2 while deposition of predominantly 6H occurred at 2623 K at 5.3×10^4 dynes/cm^2, on [0001] oriented 6H-SiC substrates (Kanaya et al., 1991).

These studies demonstrate that the range of growth temperatures (e.g., lowest growth temperature) for a SiC polytype depends on both the synthesis process and physical parameters. However, certain conditions, such as the ratio of available Si/C in the gas (Fissel, 2000) or the preparation of the substrate (Matsunami, 1993), are reported to favor, for example, 6H over 3C SiC growth. Although temperatures in the above cited experiments cannot be directly compared because of differences in the experimental setups, distinct trends are present. Hexagonal 2H is the lowest temperature SiC polytype in stability and growth temperature. As temperature is increased, the next SiC polytype to form is 3C. If temperature is increased further, 2H SiC formation will cease. Cubic 3C SiC has a wide range of growth temperatures and as temperature is increased further, the general trend in the collective studies is that higher order SiC polytypes begin to grow along with 3C SiC, until temperatures exceed the 3C formation range. In this respect, 2H and 3C can be considered the lowest temperature SiC polytypes.

Equilibrium thermochemical calculations have been performed that thoroughly map the parameter space of P, T, and C/O (Sharp and Wasserburg, 1995; Lodders and Fegley, 1995), and can be used to predict condensation sequences and initial condensation temperatures for various presolar grain species in carbon star envelopes. These calculations necessarily assume that chemical equilibrium is reached in the grain formation environment. It has been argued that gas-grain equilibrium is approached near the AGB stellar photosphere where high temperature condensates form, based on the good agreement between observed and predicted mineral species (Bernatowicz et al., 1996) as well as on trace element abundance patterns in circumstellar SiC (Amari et al., 1995b; Lodders and Fegley, 1997).

The mineral species that condense from stellar envelopes depend critically on the gas C/O ratio. The CO molecule readily forms in circumstellar shells and is the most strongly bonded diatomic molecule which is not easily disassociated. Therefore, only when C/O >1 will carbon be available for graphite and carbides to condense. Some further constraints on condensation pressures, temperatures, and C/O ratios in carbon star atmospheres can be obtained from the inferred condensation sequence of various carbon-bearing presolar minerals. Bernatowicz et al. (1996) found that the refractory carbide TiC as well as

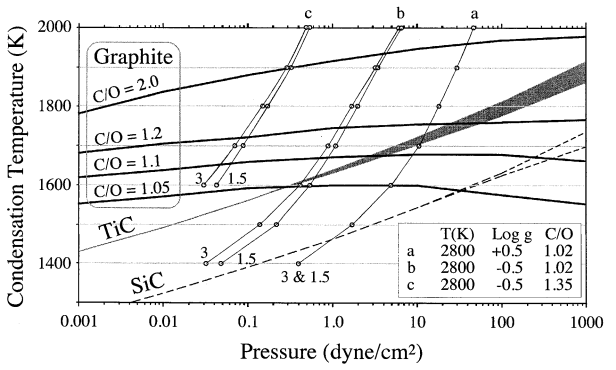

Fig. 14. Equilibrium condensation temperatures for TiC, SiC, and graphite as functions of total gas pressure and C/O ratio, in a gas of solar metallicity except for C abundance (data from Lodders and Fegley, 1995). The calculations of Lodders and Fegley (1995) showed that 3C SiC is more stable than 6H SiC under the T and P conditions considered, and the data reported by them were results from calculations that used the thermodynamic parameters for 3C SiC (K. Lodders, private communication). The minerals plotted are stable below their condensation temperature. Carbide condensation temperatures are displayed as envelopes, with the lower boundary of the envelope for C/O = 1.05 and the upper boundary for C/O $\geq$1.2. For graphite, the condensation temperature is rather insensitive to pressure but strongly dependent on C/O, but for TiC and SiC the opposite is true. Curves labeled **a, b** and **c** are model P-T profiles for atmospheres of low mass AGB carbon stars of 1.5 and 3 times $M_{\odot}$ having solar metallicity (except for enhanced C) and an effective (i.e., photospheric) temperature of 2800 K (from the spherical geometry simulations of Jørgensen et al., 1992). Curves **a** and **b** are for carbon stars with C/O = 1.02 at two different values of the surface gravity g, whose values are shown in the legend as the logarithm of the acceleration in cgs units. Curves **a** (Log g = +0.5) correspond to photospheric radius R=160–115 $R_{\odot}$ (for 3–1.5 $M_{\odot}$, respectively), and curves **b** (Log g = −0.5) correspond to photospheric radius R=510–360 $R_{\odot}$. Curves **c** are for the same physical parameters as curves **b**, except for elevated C/O = 1.35, showing that increasing C/O shifts the temperature profile to lower pressures for any given temperature.

solid solutions of TiC, MoC and the very refractory carbide ZrC often occur within presolar graphite spherules. They inferred that formation of Ti, Mo, and Zr carbide solid solutions preceded graphite formation, because frequently these refractory carbides are located in the center of graphite spherules and clearly served as nucleation sites for graphite condensation. In comparison, despite the many sectioned graphite grains examined to date (e.g., see Croat et al., 2002), SiC was only once observed to occur within graphite (Bernatowicz et al., 1996). The implied *typical* formation sequence is therefore TiC condensation (and TiC, MoC, ZrC solid solutions), followed by graphite condensation, and finally by SiC condensation.

As shown in Figure 14, the condensation temperatures of TiC and SiC are insensitive to the C/O ratio, but are strongly dependent on total gas pressure. On the other hand, the condensation temperature of graphite is rather insensitive to the total gas pressure, but is strongly dependent on the C/O ratio. This fortunate circumstance permits constraints to be placed on these various parameters by reference to the inferred condensation sequence. For example, if the C/O ratio is ~1.5, condensation of TiC before graphite can only occur at pressures >1000 dyne/cm^2. Pressures of this magnitude are characteristic of photospheres of carbon stars, however most photospheric temperatures (mean 2650 K, σ = 250 K) are far too high for any grains to condense (cf. Lodders and Fegley, 1995 and references therein). Lower C/O ratios and lower pressures are therefore required to produce the observed condensation sequence of TiC ->graphite, with plausible values in the range 1.2 $\geq$C/O >1.0 and $p <$ ~100 dyne/cm^2 (Bernatowicz et al., 1996). In comparison, the distribution of C/O ratios of carbon stars inferred from astronomical observations is relatively sharply peaked with a median of C/O = 1.1 and σ = 0.16 (Lambert et al., 1986 cf. Lodders and Fegley, 1995). Although a few carbon stars were reported to have C/O >1.4, the majority of the carbon star population is consistent with the C/O range suggested by the inferred grain condensation sequence. It is likewise consistent with the observational requirement that SiC condensation must follow the condensation of graphite (for $p <$ 100 dyne/cm^2, ~1.1 >C/O >1, as inferred by Sharp and Wasserburg, 1995). Grain formation must therefore be restricted to the stellar atmosphere, at distances greater than the photospheric radius, where temperatures tend to fall off rather rapidly. Figure 14 shows some model temperature profiles for atmospheres of low (1.5–3 × solar) mass carbon AGB stars (Jørgensen et al., 1992). It is seen that several model temperature profiles indeed produce the observed sequence TiC -> graphite -> SiC, provided that the C/O ratio does not much exceed unity.

The temperature range for SiC condensation in the majority of carbon stars can be estimated from Figure 14 (i.e., Sharp and Wasserburg, 1995; Lodders and Fegley, 1995) by using C/O = 1.1 (the median ratio inferred from astronomical observation) and by assuming that the inferred mineral condensation sequence (TiC -> graphite -> SiC) discussed previously is characteristic of the majority population of carbon stars. These assumptions predict that grain condensation occurs between total gas pressures of 3–300 dynes/cm^2. In this pressure range, the predicted temperatures for equilibrium SiC condensation are ~ 1500–1670 K. A slightly lower C/O= 1.05 predicts grain condensation at pressures of 0.3–30 dynes/cm^2 and SiC condensation between ~ 1422–1590 K. Even for C/O = 1.20, predicted SiC condensation temperatures are constrained to be no greater than 1770 K. Condensation temperatures predicted by the chemical equilibrium calculations represent the temperature at which vapor and condensates coexist in equilibrium; however, because of the effect of undercooling the actual condensation temperatures can be somewhat lower.

It is important to emphasize that these relatively low condensation temperatures are a direct consequence of the low pressures in AGB atmospheres predicted from the inferred condensation sequence of minerals (TiC -> graphite -> SiC), and that these low temperatures undoubtedly play an important role in the kinds of polytype structures that are ultimately produced. Temperatures at which 2H SiC are known to grow and remain stable, ~1473–1723 K, (Patrick et al., 1966; Krishna et al., 1971; Stan et al., 1994) largely fall within the range predicted for SiC formation in most circumstellar atmospheres by equilibrium thermodynamics (Sharp and Wasserburg, 1995; Lodders and Fegley, 1995). Additionally, in the very same experiments that synthesized 2H SiC the formation of predominantly 3C SiC was observed at temperatures >1700 K (Patrick et al., 1966). Formation of 3C SiC in those experiments occurs slightly above the temperature range predicted for SiC condensation in AGB stars, but the agreement is per-

haps as good as can be expected from laboratory experiments that may only approximate the formation conditions and gas compositions appropriate for AGB atmospheres. Nonetheless, as previously discussed, all of the higher order SiC polytypes are only known to form at temperatures *higher* than that of 3C SiC under similar conditions for a given vapor condensation process. This plausibly explains why only two polytypes (2H and 3C) out of a possible order of a hundred different kinds are observed in presolar SiC.

Mass outflows in AGB atmospheres are often characterized in terms of spherically symmetric, smoothly varying spatial functions of T, P, and composition (e.g., see, Cherchneff et al., 1992; Cadwell et al., 1994; Chigai et al., 1999). However, there is considerable evidence that the mass outflows are considerably more complicated than depicted in such models, and in fact are often clumpy and frequently depart from spherical symmetry (e.g., Olofsson, 1996; Weigelt et al., 1998). Fortunately, to construct a tentative framework in which to interpret the observational results presented here, we need not be concerned with the global aspects of stellar atmosphere mass outflows. We need only to consider the progressive physical and chemical changes in a representative parcel of gas within the mass outflow. We therefore make the simplifying assumption that the parcel behaves as a closed system as it moves outward from a location close to the stellar photosphere to locations at larger radii. Neglecting any consideration of the specific rate at which this transport occurs (and thus about the kinetics of grain growth), or how transport rates may vary among parcels, we simply assume that as a parcel moves outward it expands adiabatically. Consequently, its temperature decreases monotonically with time, and the number density of gas contributing to grain growth in the parcel also decreases (at a rate faster than the temperature). These changes induce the parcel to evolve chemically. Although we can hardly expect this general picture to depict the grain formation process in detail, we do expect that the inferred polytype formation sequence and required physical conditions will be broadly correct.

In regard to the majority population of carbon stars ($1 < C/O < 1.2$), the typical sequence of mineral condensation (TiC ->graphite ->SiC) inferred from the laboratory study of presolar grains and interpreted with the aid of equilibrium thermodynamics, leads to the conclusion that relatively low pressures prevail in the regions of circumstellar atmospheres where the grains condense. This conclusion is essentially independent of any stellar atmosphere model. The equilibrium condensation behavior of SiC (Fig. 14) shows that at these low pressures, the formation of SiC can only occur at relatively low temperatures that are considerably less than the experimental formation temperatures of most SiC polytypes. Indeed, comparison of these equilibrium thermodynamic temperatures with experimental data on the formation of SiC polytypes leads to the conclusion that *only* 2H and 3C polytypes are likely to grow in circumstellar atmospheres. This prediction is verified by the laboratory observations carried out in the present work. With these points in mind, we propose that close to the carbon star photosphere, photon and particle irradiation fluxes, as well as temperature, are sufficiently high to prevent nascent nucleating clusters from reaching critical size for sustained condensate growth. Therefore, there will be a "no growth region" for dust close to the star. At radii in the stellar atmosphere where the irradiation fluxes and temperatures are sufficiently low, the highest temperature condensates such as TiC and graphite can form (Sharp and Wasserburg, 1995; Lodders and Fegley, 1995). At farther radii, the highest temperature SiC polytype observed in Murchison, 3C, will be first to condense and grow. It has been argued that the 3C polytype is the most stable structure for SiC nuclei (Tairov and Tsvetkov, 1982), suggesting that 3C SiC nuclei have a higher probability of reaching critical size over nuclei of other polytypes. Higher order SiC polytypes may indeed nucleate at higher temperatures (corresponding to smaller radii) than 3C growth regions or even along side 3C SiC at the highest 3C growth temperatures, but for their growth to occur would require that these less stable SiC nuclei reach critical size, in some cases, under conditions of larger irradiation fluence. This could contribute to the lack of polytypes of order higher than 3C in circumstellar SiC. At still larger atmospheric radii, in expanded cooler gas regions with smaller irradiation fluences, the lowest temperature polytype, 2H SiC, would grow. At intermediate radii in the SiC growth region, intergrowth grains might form directly or by 2H SiC heteroepitaxial growth on preexisting 3C SiC grains which were transported to cooler regions in AGB mass outflows by stellar radiation pressure.

The observed relative frequency of occurrence of 3C and 2H SiC crystals is also consistent with the scenario outlined above. Since the rate of grain nucleation from the gas varies as the square of the number density of any gas species contributing to grain growth (McDonald, 1963), we predict that the polytypes nucleating at higher temperatures and higher gas number densities will be more abundant than polytypes nucleating later at lower temperatures and lower number densities in the expanding gas parcel. Not only will the nucleation rate of lower temperature forms of SiC be reduced because of the decreasing number density of Si in the expanding gas, but also because of the prior removal of Si into the SiC already formed at higher temperatures (cf. Lodders and Fegley, 1995). In qualitative accord with these expectations, single crystals of 3C SiC, which formed at higher temperatures than 2H SiC and therefore at higher gas phase Si number densities, are far more numerous than single crystals of 2H SiC (see Table 3).

5. SUMMARY AND CONCLUSIONS

Silicon carbide is an important species of stardust, and isotopic studies of many different elements reveal that nearly all presolar SiC was produced in low mass AGB carbon stars. Under the simple and reasonable assumption that presolar SiC in primitive meteorites is a representative sample of the sum of SiC produced by the many different types of stellar sources, a determination of the structure of presolar SiC thus translates, to first order, into a direct determination of the structure of SiC produced by AGB stars. Although IR astronomical studies detect SiC in the mass outflows from carbon stars, these studies can only distinguish between cubic SiC (β-SiC) and non-cubic SiC (all hexagonal and rhombohedral polytypes, collectively termed α-SiC), and even this crude differentiation has been controversial. Thus, the direct TEM determination of SiC crystal structure provides a reference standard that can aid in the understanding of which subset of physical properties (e.g., size,

shape, crystallographic structure) is relevant for interpreting IR spectra of SiC from carbon stars. Further, on the order of a hundred different polytypes of SiC have been synthesized in the laboratory. The particular polytypes produced in any process depend on specific physical and chemical conditions such as temperature, pressure, the composition of precursors, and (in cases of deposition) the microstructure of substrates. Therefore, the distribution of polytypes in presolar SiC is used here to evaluate models of grain formation in circumstellar atmospheres.

Our principal experimental result is that presolar SiC occurs in *only* the two simplest polytypic forms: cubic 3C (~80%) and hexagonal 2H (~3%), and intergrowths of these two forms (~17%), in addition to a small number of one-dimensionally disordered SiC grains (~0.9%). The presolar origin of at least one 2H grain is demonstrated based on the anomalous $^{12}C/^{13}C = 64 \pm 4$ (terrestrial = 89), and $^{14}N/^{15}N = 575 \pm 24$ (terrestrial = 272) isotopic composition of the grain. In fact, this is the first report of 2H SiC forming in nature. We further conclude that the measured polytype distribution reflects original growth abundances and is not altered by post-formation thermal transformation. Therefore, we interpret the observed structural simplicity as the result of the specific physical conditions in AGB circumstellar atmospheres. In particular, total gas pressures in the extended stellar atmospheres exterior to carbon star photospheres are quite low (<100 dyne/cm^2), so SiC condensation in these atmospheres is restricted to relatively low temperatures (at least several hundred degrees below 2000 K). In general, laboratory studies have shown that at these low temperatures, 2H and 3C are the most stable SiC polytypes to form in vapor condensation processes, and that for any given set of physical conditions, all SiC polytypes of higher order than 2H and 3C form at greater temperatures than those at which these two polytypes form. A simple hypothesis that accounts for the observations is that 3C SiC first condensed at small radii (high temperatures) and 2H SiC condensed at larger radii (lower temperatures) in AGB atmospheres. At intermediate radii in the SiC growth region, intergrowth grains might form directly or by 2H SiC heteroepitaxial growth on preexisting 3C SiC grains which were transported to cooler regions in AGB mass outflows by stellar radiation pressure.

Acknowledgments—We thank Dr. Robert Walker of the Laboratory for Space Sciences of Washington University for encouragement and support through the years. We thank Dr. Lynn E. Rehn and Dr. Marquis A. Kirk of the Materials Science Division of Argonne National Laboratory for encouragement. We thank summer students E. Legget and B. Blust (both funded by the George Washington University Science and Engineering Apprentice Program) for measuring SiC grain size from digitized TEM micrographs. We thank manuscript editor Dr. Ulrich Ott, reviewer Dr. R. A. Mendybaev, and anonymous reviewers for their constructive and critical reviews. This work was partially supported by DOE, NRL, NASA, and NSF.

Associate editor: U. Ott

REFERENCES

Acheson E. G. (1893) On Carborundum. *Chem. News* **68**, 179.

Addamiano A. (1982) Preparation and properties of 2H SiC crystals. *J. Cryst. Growth* **58**, 617–622.

Alexander C. M. O'D. (1993) Presolar SiC in chondrites: How variable and how many sources? *Geochim. Cosmochim. Acta* **57**, 2869–2888.

Amari S., Anders E., Virag A., and Zinner E. (1990) Interstellar graphite in meteorites. *Nature* **345**, 238–240.

Amari S., Hoppe P., Zinner E., and Lewis R. S. (1992) Interstellar SiC with unusual isotopic compositions: Grains from a supernova? *Astrophys. J.* **394**, L43–46.

Amari S., Lewis R. S., and Anders E. (1994) Interstellar grains in meteorites: I. Isolation of SiC, graphite, and diamond; size distributions of SiC and graphite. *Geochim. Cosmochim. Acta* **58**, 459–470.

Amari S., Lewis R. S., and Anders E. (1995a) Interstellar grains in meteorites: III. Graphite and its noble gases. *Geochim. Cosmochim. Acta* **59**, 1411–1426.

Amari S., Hoppe P., Zinner E., and Lewis R. S. (1995b) Trace-element concentrations in single circumstellar silicon carbide grains from the Murchison meteorite. *Meteoritics* **30**, 679–693.

Amari S., Zinner E., and Lewis R. S. (1996) Ca and Ti isotopic compositions of size-separated SiC fractions from the Murchison meteorite. *Lunar Planet. Sci.* **XXVII**, 23–24 (abs).

Amari S., Zinner E., and Lewis R. S. (2000) Isotopic compositions of different presolar silicon carbide size fractions from the Murchison meteorite. *Meteor. Planet. Sci.* **35**, 997–1014.

Amari S., Nittler L. R., Zinner E., Gallino R., Lugaro M., and Lewis R. S. (2001a) Presolar SiC grains of type Y. Origin from low-metallicity asymptotic giant branch stars. *Astrophys. J.* **546**, 248–266.

Amari S., Nittler L. R., Zinner E., Lodders K., and Lewis R. S. (2001b) Presolar SiC grains of type A, and B. Their isotopic compositions and stellar origins. *Astrophys. J.* **559**, 463–483.

Amari S., Jennings C., Nguyen A., Stadermann F. J., Zinner E., and Lewis R. S. (2002) NanoSIMS isotopic analysis of small presolar SiC grains from the Murchison and Indarch meteorites. *Lunar Planet. Sci.* **XXXIII**, 1205 (abs).

Anders E. and Zinner E. (1993) Interstellar grains in primitive meteorites: Diamond, silicon carbide, and graphite. *Meteoritics* **28**, 490–514.

Andersen A. C., Jäger C., Mutschke H., Braatz A., Clément D., Henning Th., Jørgensen U. G., and Ott U. (1999) Infrared spectra of meteoritic SiC grains. *Astron. Astrophys.* **343**, 933–938.

Baumhauer H. (1912) Uber die kristalle des carborundums. *Z. Krist.* **50**, 33–39.

Baumhauer H. (1915) Uber die verschiedenen modifikationen des carborundums und die erscheinung der poytypie. *Z. Krist.* **55**, 249–259.

Bender H., De Veirman A., Van Landuyt J., and Amelinckx S. (1986) HREM investigation of twinning in very high dose phosphorus ion-implanted silicon. *Appl. Phys. A* **39**, 83–90.

Berman I. and Ryan C. E. (1971) The growth of silicon carbide needles by the vapor-liquid-solid method. *J. Cryst. Growth* **9**, 314–318.

Bernatowicz T. J., Amari S., Zinner E. K., and Lewis R. S. (1991) Interstellar grains within interstellar grains. *Astrophys. J.* **373**, L73–L76.

Bernatowicz T., Fraundorf G., Tang† M., Anders E., Wopenka B., Zinner E., and Fraundorf P. (1987) Evidence for interstellar SiC in the Murray carbonaceous meteorite. *Nature* **330,** 728–730.

Bernatowicz T. J., Cowsik R., Gibbons P. C., Lodders K., Fegley B. Jr., Amari S., and Lewis R. S. (1996) Constraints on stellar grain formation from presolar graphite in the Murchison meteorite. *Astrophys. J.* **472**, 760–782.

Bernatowicz T., Bradley J., Amari S., Messenger S., and Lewis R. (1999) New kinds of massive star condensates in a presolar graphite from Murchison. *Lunar Planet. Sci.* **XXX**, 1392 (abs).

Blanco A., Borghesi A., Fonti S., and Orofino V. (1994) Amorphous carbon and silicon carbide grain mixtures in the envelopes of carbon stars. *Astron. Astrophys.* **283**, 561–566.

Blanco A., Borghesi A., Fonti S., and Orofino V. (1998) Circumstellar emission from dust envelopes around carbon stars showing the silicon carbide feature. *Astron. Astrophys.* **330**, 505–514.

Bootsma G. A., Knippenberg W. F., and Verspui G. (1971) Phase transformations, habit changes and crystal growth in SiC. *J. Cryst. Growth* **8**, 341–353.

Cadwell B. J., Wang H., Feigelson E. D., and Frenklach M. (1994) Induced nucleation of carbon dust in red giant stars. *Astrophys. J.* **429**, 285–299.

Cherchneff I., Barker J. R., and Tielens A. G. G. M. (1992) Polycyclic aromatic hydrocarbon formation in carbon-rich stellar envelopes. *Astrophys. J.* **401**, 269–287.

Chigai T., Yamamoto T., and Kozasa T. (1999) Formation conditions of presolar TiC core-graphite mantle spherules in the Murchison meteorite. *Astrophys. J.* **510**, 999–1010.

Choi B.-G., Wasserburg G. J., and Huss G. R. (1999) Circumstellar hibonite and corundum and nucleosynthesis in asymptotic giant branch stars. *Astrophys. J.* **522**, L133–L136.

Clayton D. D. (1997) Placing the sun and mainstream SiC particles in galactic chemodynamic evolution. *Astrophys. J.* **484**, L67–L70.

Clayton D. D. and Ward R. A. (1978) s-Process studies: Xenon and krypton isotopic abundances. *Astrophys. J.* **224**, 1000–1006.

Cowley J. M. and Moodie A. F. (1957) The scattering of electrons by atoms and crystals. I. A new theoretical approach. *Acta Cryst.* **10**, 609–619.

Croat K., Bernatowicz T., Stadermann F. J., Messenger S., and Amari S. (2002) Coordinated isotopic and TEM studies of a supernova graphite. *Lunar Planet. Sci.* **XXXIII**, 1315 (abs).

Daulton T. L. (1992) The quasicrystalline decagonal and related crystalline approximant structures. Ph.D. dissertation thesis, Washington University in St. Louis.

Daulton T. L., Eisenhour D. D., Bernatowicz T. J., Lewis R. S., and Buseck P. R. (1996) Genesis of presolar diamonds: Comparative high-resolution transmission electron microscopy study of meteoritic and terrestrial nano-diamonds. *Geochim. Cosmochim. Acta* **60**, 4853–4872.

Daulton T. L., Bernatowicz T. J., Lewis R. S., Messenger S., Stadermann F. J., and Amari S. (2002) Polytype Distribution in Circumstellar Silicon Carbide. *Science* **296**, 1852–1855.

Dorignac D., Serin V., Delclos S., Phillipp F., Rats D., and Vandenbulcke L. (1997) HREM and EXELFS investigation of local structure in thin CVD diamond films. *Diam. Rel. Mater.* **6**, 758–762.

Fissel A. (2000) Thermodynamic considerations of the epitaxial growth of SiC polytypes. *J. Cryst. Growth* **212**, 438–450.

Forrest W. J., Gillett F. C., and Stein W. A. (1975) Circumstellar grains and the intrinsic polarization of starlight. *Astrophys. J.* **195**, 423–440.

Friedemann Chr. (1969) Evolution of silicon carbide particles in the atmospheres of carbon stars. *Physica* **41**, 139–143.

Gallino R., Raiteri C. M., Busso M., and Matteucci F. (1994) The puzzle of silicon, titanium, and magnesium anomalies in meteoritic silicon carbide grains. *Astrophys. J.* **430**, 858–869.

Gallino R., Busso M., and Lugaro M. (1997) Neutron capture nucleosynthesis in AGB stars. In *Astrophysical Implications of the Laboratory Study of Presolar Materials* (eds. T. J. Bernatowicz and E. K. Zinner), pp. 115–153. AIP, New York.

Gilman R. C. (1969) On the composition of circumstellar grains. *Astrophys. J.* **155**, L185–L187.

Groenewegen M. A. T. (1995) Dust shells around infrared carbon stars. *Astron. Astrophys.* **293**, 463–478.

Henning Th. and Mutschke H. (2001) Formation and spectroscopy of carbides. *Spectrochim. Acta Part A* **57**, 815–824.

Hoppe P. and Ott U. (1997) Mainstream silicon carbide grains from meteorites. In *Astrophysical Implications of the Laboratory Study of Presolar Materials* (eds. T. J. Bernatowicz and E. K. Zinner), pp. 27–58. AIP, New York.

Hoppe P., Strebel R., Eberhardt P., Amari S., and Lewis R. S. (1993) Interstellar SiC: Extended studies of C, N, and Si isotopes in small single grains. *Meteoritics* **28**, 363–364 (abs).

Hoppe P., Strebel R., Eberhardt P., Amari S., and Lewis R. S. (1994a) Evidence for an interstellar nitride grain with highly anomalous isotopic compositions of C, N and Si. *Lunar Planet. Sci.* **XXV**, 563–564 (abs).

Hoppe P., Amari S., Zinner E., Ireland T., and Lewis R. S. (1994b) Carbon, nitrogen, magnesium, silicon, and titanium isotopic compositions of single interstellar silicon carbide grains from the Murchison carbonaceous chondrite. *Astrophys. J.* **430**, 870–890.

Hoppe P., Strebel R., Eberhardt P., Amari S., and Lewis R. S. (1996a) Small SiC grains and a nitride grain of circumstellar origin from the Murchison meteorite: Implications for stellar evolution and nucleosynthesis. *Geochim. Cosmochim. Acta* **60**, 883–907.

Hoppe P., Strebel R., Eberhardt P., Amari S., and Lewis R. S. (1996b) Type II supernova matter in a silicon carbide grain from the Murchison meteorite. *Science* **272**, 1314–1316.

Hoppe P., Annen P., Strebel R., Eberhardt P., Gallino R., Lugaro M., Amari S., and Lewis R. S. (1997) Meteoritic silicon carbide grains with unusual Si-isotopic compositions: Evidence for an origin in low-mass, low-metallicity asymptotic giant branch stars. *Astrophys. J.* **487**, L101–L104.

Hoppe P., Kocher Th., Eberhardt P., Amari S., and Lewis R. S. (1998) Carbon- and nitrogen-isotopic compositions of individual, submicrometer-sized presolar silicon carbide grains. *Meteor. Planet. Sci.* **33**, A71 (abs).

Huss G. R. (1997) The survival of presolar grains in solar system bodies. In *Astrophysical Implications of the Laboratory Study of Presolar Materials* (eds. T. J. Bernatowicz and E. K. Zinner), pp. 721–748. AIP, New York.

Huss G. R. and Lewis R. S. (1995) Presolar diamond, SiC, and graphite in primitive chondrites: Abundances as a function of meteorite class and petrologic type. *Geochim. Cosmochim. Acta* **59**, 115–160.

Huss G. R., Fahey A. J., Gallino R., and Wasserburg G. J. (1994) Oxygen isotopes in circumstellar Al_2O_3 grains from meteorites and stellar nucleosynthesis. *Astrophys. J.* **430**, L81–L84.

Hutcheon I. D., Huss G. R., Fahey A. J., and Wasserburg G. J. (1994) Extreme ^{26}Mg and ^{17}O enrichments in an Orgueil corundum: Identification of a presolar oxide grain. *Astrophys. J.* **425**, L97–L100.

Ireland T. R., Zinner E. K., and Amari S. (1991) Isotopically anomalous Ti in presolar SiC from the Murchison meteorite. *Astrophys. J.* **376**, L53–L56.

Jagodzinski H. (1954) Polytypism in SiC crystals. *Acta Cryst.* **7**, 300.

Jaques A. L., Hall A. E., Sheraton J. W., Smith C. B., Sun S. S., Drew R. M., Foudoulis C., and Ellingsen K. (1989) Composition of crystalline inclusions and C-isotopic composition of Argyle and Ellendale diamonds. In *Kimberlites and Related Rocks Volume 2: Their mantle/Crust Setting, Diamond and Diamond Exploration* (eds. J. Ross, A. L. Jaques, J. Ferguson, D. H. Green, S. Y. O'Reily, R. V. Danchin, and A. J. A. Janse), pp. 966–989. Blackwell Scientific, Cambridge.

Jørgensen U. G., Johnson H. R., and Nordlund Å. (1992) Effects of sphericity in carbon star atmospheres. *Astron. Astrophys.* **261**, 263–273.

Kaminskiy F. V., Bukin V. I., Potapov S. V., Arkus N. G., and Ivanova V. G. (1969) Discoveries of silicon carbide under natural conditions and their genetic importance. *Intern. Geol. Rev.* **11**, 561–569.

Kanaya M., Takahashi J., Fujiwara Y., and Moritani A. (1991) Controlled sublimation growth of single crystalline 4H-SiC and 6H-SiC and identification of polytypes by X-ray diffraction. *Appl. Phys. Lett.* **58**, 56–58.

Kern R. S., Tanaka S., Rowland L. B., and Davis R. F. (1998) Reaction kinetics of silicon carbide deposition by gas-source molecular-beam epitaxy. *J. Cryst. Growth* **183**, 581–593.

Kimoto T., Nishino H., Yoo W. S., and Matsunami H. (1993) Growth mechanism of 6H-SiC in step-controlled epitaxy. *J. Appl. Phys.* **73**, 726–732.

Knippenberg W. F. (1963) Growth phenomena in silicon carbide. *Philips Res. Rep.* **18**, 161–274.

Krishna P. and Marshall R. C. (1971a) The structure, perfection and annealing behaviour of SiC needles grown by a VLS mechanism. *J. Cryst. Growth.* **9**, 319–325.

Krishna P. and Marshall R. C. (1971b) Direct transformation from the 2H to the 6H structure in single-crystal silicon carbide. *J. Cryst. Growth* **11**, 147–150.

Krishna P., Marshall R. C., and Ryan C. E. (1971) The discovery of a 2H-3C solid state transformation in silicon carbide single crystals. *J. Cryst. Growth* **8**, 129–131.

Lambert D. L., Gustafsson B., Eriksson K., and Hinkle K. H. (1986) The chemical composition of carbon stars: I. Carbon, nitrogen, and oxygen in 30 cool carbon stars in the galactic disk. *Astrophys. J. Suppl.* **62**, 373–425.

Lely J. A. (1955) Darstellung von Einkristallen von Siliciumcarbid und Beherrschung von Art und Menge der eingebauten Verunreinigungen. *Ber. Deut. Keram. Ges.* **32**, 229–231.

Leung I. S. (1990) Silicon carbide cluster entrapped in a diamond from Fuxian, China. *Am. Mineral.* **75**, 1110–1119.

Leung I., Guo W., Friedman I., and Gleason J. (1990a) Natural occurrence of silicon carbide in a diamondiferous kimberlite from Fuxian. *Nature* **346**, 352–354.

Leung I., Guo W., Friedman I., and Gleason J. (1990b) Correction: Natural occurrence of silicon carbide in a diamondiferous kimberlite from Fuxian. *Nature* **346**, 874.

Lewis R. S., Tang† M., Wacker J. F., Anders E., and Steel E. (1987) Interstellar diamonds in meteorites. *Nature* **326**, 160–162.

Lewis R. S., Amari S., and Anders E. (1990) Meteoritic silicon carbide: pristine material from carbon stars. *Nature* **348**, 293–298.

Lewis R. S., Amari S., and Anders E. (1994) Interstellar grains in meteorites: II. SiC and its noble gases. *Geochim. Cosmochim. Acta* **58**, 471–494.

Lodders K. and Fegley B. Jr. (1995) The origin of circumstellar silicon carbide grains found in meteorites. *Meteoritics* **30**, 661–678.

Lodders K. and Fegley B. Jr. (1997) Complementary trace element abundances in meteoritic SiC grains and carbon star atmospheres. *Astrophys. J.* **484**, L71–L74.

Lodders K. and Fegley B. Jr. (1998) Presolar silicon carbide grains and their parent stars. *Meteor. Planet. Sci.* **33**, 871–880.

Lugaro M., Zinner E., Gallino R., and Amari S. (1999) Si isotopic ratios in mainstream presolar SiC grains revisited. *Astrophys. J.* **527**, 369–394.

Lyakhovich V. V. (1980) Origin of accessory moissanite. *Intern. Geol. Rev.* **22**, 961–970.

Mathez E. A., Fogel R. A., Hutcheon I. D., and Marshintsev V. K. (1995) Carbon isotopic composition and origin of SiC from kimberlites of Yakutia, Russia. *Geochim. Cosmochim. Acta* **59**, 781–791.

Marshintsev V. K., Zayakina N. V., and Leskova N. V. (1982) New find of cubic silicon carbide, as inclusions in moissanite from kimberlitic rocks. *Trans. Dokl. U. S. S. R. Acad. Sci: Earth Sci. Sect.* **262**, 163–166.

Mason B. (1967) Extraterrestrial mineralogy. *Am. Mineral.* **52**, 307–325.

Matsunami H. (1993) Progress in epitaxial growth of SiC. *Physica B* **185**, 65–74.

McDonald J. E. (1963) Homogeneous nucleation of vapor condensation II: Kinetic aspects. *Am. J. Phys.* **31**, 31–41.

Mendybaev R. A., Beckett J. R., Grossman L., Stolper E., Cooper R. F., and Bradley J. P. (2002) Volatilization kinetics of silicon carbide in reducing gases: An experimental study with applications to the survival of presolar grains in the solar nebula. *Geochim. Cosmochim. Acta* **66**, 661–682.

Merz K. M. and Adamsky R. F. (1959) Synthesis of the wurtzite form of silicon carbide. *J. Am. Chem. Soc.* **81**, 250–251.

Milton C. and Vitaliano D. B. (1985) Moissanite SiC, a geological aberration. *98th Ann. Meeting, The Geological Society of America, October 28–31, 1985, Orlando Florida* 665 (abs).

Moissan H. (1905) Étude du siliciure de carbone de la météorite Canon Diablo. *Comptes rendus Acad. sci.* **140**, 405–506.

Moore R. O. and Gurney J. J. (1989) Mineral inclusions in diamond from Monastery kimberlite, South Africa. In *Kimberlites and Related Rocks Volume 2: Their mantle/Crust Setting, Diamond and Diamond Exploration* (eds. J. Ross, A. L. Jaques, J. Ferguson, D. H. Green, S. Y. O'Reily, R. V. Danchin, and A. J. A. Janse), pp. 1029–1041. Blackwell Scientific, Cambridge.

Moore R. O., Otter M. L., Rickard R. S., Harris J. W., and Gurney J. J. (1986) The occurrence of moissanite and ferro-periclase as inclusions in diamond. In *4th International Kimberlite Conference, Perth, Extended Abstracts; Abstr. Geol. Soc. Australia* **16**, pp. 409–411 (abs).

Mutschke H., Andersen A. C., Clément D., Henning Th., and Peiter G. (1999) Infrared properties of SiC particles. *Astron. Astrophys.* **345**, 187–202.

Narayan J. (1990) Dislocations, twins, and grain boundaries in CVD diamond thin films: Atomic structure and properties. *J. Mater. Res.* **5**, 2414–2423.

Nicolussi G. K., Davis A. M., Pellin M. J., Lewis R. S., Clayton R. N., and Amari S. (1997) s-Process zirconium in presolar silicon carbide grains. *Science* **277**, 1281–1283.

Nicolussi G. K., Pellin M. J., Lewis R. S., Davis A. M., Amari S., and Clayton R. N. (1998) Molybdenum isotopic composition of individual presolar silicon carbide grains from the Murchison meteorite. *Geochim. Cosmochim. Acta* **62**, 1093–1104.

Nittler L. R. and Alexander C. M. O'D. (1999) Automatic identification of presolar Al- and Ti-rich oxide grains from ordinary chondrites. *Lunar Planet. Sci.* **XXX**, 2041 (abs).

Nittler L. R., Alexander C. M. O'D., Gao X., Walker R. M., and Zinner E. K. (1994) Interstellar oxide grains from the Tieschitz ordinary chondrite. *Nature* **370**, 443–446.

Nittler L. R., Hoppe P., Alexander C. M. O'D., Amari S., Eberhardt P., Gao X., Lewis R. S., Strebel R., Walker R. M., and Zinner E. (1995) Silicon nitride from supernovae. *Astrophys. J.* **453**, L25–L28.

Olofsson H. (1996) Circumstellar molecular envelopes of AGB and post-AGB objects. *Astrophys. Space Sci.* **245**, 169–200.

Ott U. and Begemann F. (1990) Discovery of *s*-process barium in the Murchison meteorite. *Astrophys. J.* **353**, L57–L60.

Otter M. L. and Gurney J. J. (1989) Mineral inclusions in diamond from the Sloan diatreme, Colorado-Wyoming State Line kimberlite district, North America. In *Kimberlites and Related Rocks Volume 2: Their mantle/Crust Setting, Diamond and Diamond Exploration* (eds. J. Ross, A. L. Jaques, J. Ferguson, D. H. Green, S. Y. O'Reily, R. V. Danchin, and A. J. A. Janse), pp. 1042–1053. Blackwell Scientific, Cambridge.

Papoular R., Cauchetier M., Begin S., and LeCaer G. (1998) Silicon carbide and the 11.3-μm feature. *Astron. Astrophys.* **329**, 1035–1044.

Patrick L., Hamilton D. R., and Choyke W. J. (1966) Growth, luminescence, selection rules, and lattice sums of SiC with wurtzite structure. *Phys. Rev.* **143**, 526–536.

Podosek F. A., Prombo C. A., Amari S., and Lewis R. S. (2002) s-. Process isotopic compositions in presolar SiC from the Murchison meteorite. *Astrophys. J.* (in press).

Powell J. A. (1969) Crystal growth of 2H silicon carbide. *J. Appl. Phys.* **40**, 4660–4662.

Prombo C. A., Podosek F. A., Amari S., and Lewis R. S. (1993) s-Process Ba isotopic compositions in presolar SiC from the Murchison meteorite. *Astrophys. J.* **410**, 393–399.

Ramsdell L. S. (1947) Studies on silicon carbide. *Am. Mineral.* **32**, 64–82.

Randle V. (1993) The Measurement of Grain Boundary Geometry, pp. 33–45. Institute of Physics Publishing, Philadelphia.

Ranganathan S. (1966) On the geometry of coincident-site lattices. *Acta Cryst.* **21**, 197–199.

Regis A. J. and Sand L. B. (1958) Natural cubic (β) silicon carbide. *Geol. Soc. Am. Bull.* **69**, 1633 (abs).

Shaffer P. T. B. (1969) A review of the structure of silicon carbide. *Acta Cryst.* **B25**, 477–488.

Sharp C. M. and Wasserburg G. J. (1995) Molecular equilibria and condensation temperatures in carbon-rich gases. *Geochim. Cosmochim. Acta* **59**, 1633–1652.

Speck A. K., Barlow M. J., and Skinner C. J. (1997) The nature of the silicon carbide in carbon star outflows. *MNRAS.* **288**, 431–456.

Speck A. K., Hofmeister A. M., and Barlow M. J. (1999) The SiC problem: Astronomical and meteoritic evidence. *Astrophy. J.* **513**, L87–L90.

Srinivasan B. and Anders E. (1978) Noble gases in the Murchison meteorite: possible relics of s-process nucleosynthesis. *Science* **201**, 51–56.

Stan M. A., Patton M. O., Warner J. D., Yang J. W., and Pirouz P. (1994) Growth of 2H-SiC on 6H-SiC by pulsed laser ablation. *Appl. Phys. Lett.* **64**, 2667–2669.

Stroud R. M., O'Grady M., Nittler L. R., and Alexander C. M. O'D. (2002) Transmission electron microscopy of an in situ presolar silicon carbide grain. *Lunar Planet. Sci.* **XXXIII**, 1785 (abs).

Tairov Y. M. and Tsvetkov V. F. (1978) Investigation of growth processes of ingots of silicon carbide single crystals. *J. Cryst. Growth* **43**, 209–212.

Tairov Y. M. and Tsvetkov V. F. (1982) Process in controlling the growth of polytypic crystals. In *Progress in Crystal Growth and Characterization* (ed. P. Krishna), pp. 111–162. Oxford, New York, Pergamon Press.

Tang† M. and Anders E. (1988) Isotopic anomalies of Ne, Xe, and C in meteorites. II. Interstellar diamond and SiC: Carriers of exotic noble gases. *Geochim. Cosmochim. Acta* **52**, 1235–1244.

Tang† M., Anders E., Hoppe P., and Zinner E. (1989) Meteoritic silicon carbide and its stellar sources; implications for galactic chemical evolution. *Nature* **339**, 351–354.

Thibault N. W. (1944) Morphological and structural crystallography and optical properties of silicon carbide. *Am. Mineral.* **29**, 249–278.

Timmes F. X. and Clayton D. D. (1996) Galactic evolution of silicon isotopes: Application to presolar SiC grains from meteorites. *Astrophys. J.* **472**, 723–741.

Treffers R. and Cohen M. (1974) High-resolution spectra of cool stars in the 10- and 20- micron regions. *Astrophys. J.* **188**, 545–552.

Vetter W. M., Huang W., Neudeck P., Powell J. A., and Dudley M. (2001) Synchrotron white-beam topographic studies of 2H-SiC crystals. *J. Cryst. Growth* **224**, 269–273.

Verma A. R. and Krishna P. (1966) Silicon carbide and other polytypic substances. In *Polymorphism and Polytypism in Crystals*, pp. 92–135. John Wiley & Sons, New York.

Virag A., Wopenka B., Amari S., Zinner E., Anders E., and Lewis R. S. (1992) Isotopic, optical, and trace element properties of large single SiC grains from the Murchison meteorite. *Geochim. Cosmochim. Acta* **56**, 1715–1733.

Weigelt G., Balega Y., Blöcker T., Fleischer A. J., Osterbart R., and Winters J. M. (1998) 76 mas speckle-masking interferometry of IRC +10 216 with the SAO 6 m telescope: Evidence for a clumpy shell structure. *Astron. Astrophys.* **333**, L51–L54.

Wells A. F. (1950) Structural Inorganic Chemistry. Oxford University Press, Oxford.

Woolf N. J. and Ney E. P. (1969) Circumstellar infrared emission from cool stars. *Astrophys. J.* **155**, L181–L184.

Woosley S. E. and Weaver T. A. (1995) The evolution and explosion of massive stars. II. Explosive hydrodynamics and nucleosynthesis. *Astrophys. J. Suppl.* **101**, 181–235.

Wyckoff R. W. G. (1963) Crystal Structures, Vol. 1. Interscience, New York.

Yoo W. S. and Matsunami H. (1991) Polytype-controlled single-crystal growth of silicon carbide using 3C -> 6H solid-state phase transformation. *J. Appl. Phys.* **70**, 7124–7131.

Yuan C., Steckl A. J., Chaudhuri J., Thokala R., and Loboda M. J. (1995) Reduced temperature growth of crystalline 3C-SiC films on 6H-SiC by chemical vapor deposition from silacyclobutane. *J. Appl. Phys.* **78**, 1271–1273.

Zhdanov G. S. (1945) The numerical symbol of close packing of spheres and its application in the theory of close packings. *Compt. Rend. Acad. Sci. USSR.* **48**, 39–42.

Zinner E., Tang† M., and Anders E. (1987) Large isotopic anomalies of Si, C, N and noble gases in interstellar silicon carbide from the Murray meteorite. *Nature* **330**, 730–732.

Zinner E., Tang† M., and Anders E. (1989) Interstellar SiC in the Murchison and Murray meteorites: Isotopic composition of Ne, Xe, Si, C, and N. *Geochim. Cosmochim. Acta* **53**, 3273–3290.

Zinner E., Amari S., Anders E., and Lewis R. (1991a) Large amount of extinct ^{26}Al in interstellar grains from the Murchison meteorite. *Nature* **349**, 51–54.

Zinner E., Amari S., and Lewis R. S. (1991b) s-Process Ba, Nd, and Sm in presolar SiC from the Murchison meteorite. *Astrophys. J.* **382**, L47–L50.

Zinner E., Amari S., Messenger S., Nguyen A., Stadermann F. J., Walker R. M., and Lewis R. S. (2001a) Isotopic analysis of small presolar SiC grains with the NanoSIMS ion microprobe. *Meteor. Planet. Sci.* **36**, A231 (abs).

Zinner E., Amari S., Gallino R., and Lugaro M. (2001b) Presolar SiC from parent stars of varying metallicity and the galactic evolution of the Si isotopes. *Lunar Planet. Sci.* **XXXII**, 1677 (abs).

† M. Tang appears as T. Ming in the author list of the cited journals and in publication databases.